





# *Staphylococcus aureus* ATP Synthase Promotes Biofilm Persistence by Influencing Innate Immunity

Megan E. Bosch,<sup>a\*</sup> Blake P. Bertrand,<sup>a</sup> Cortney E. Heim,<sup>a</sup> Abdulelah A. Alqarzaee,<sup>a</sup> Sujata S. Chaudhari,<sup>a</sup> Amy L. Aldrich,<sup>a\*</sup> Paul D. Fey,<sup>a</sup>  Vinai C. Thomas,<sup>a</sup>  Tammy Kielian<sup>a</sup>

<sup>a</sup>Department of Pathology and Microbiology, University of Nebraska Medical Center, Omaha, Nebraska, USA

Megan E. Bosch and Blake P. Bertrand contributed equally to this study. Author order was determined both by who initiated the work and the number of figures generated by each author.

**ABSTRACT** *Staphylococcus aureus* is a major cause of prosthetic joint infection (PJI), which is characterized by biofilm formation. *S. aureus* biofilm skews the host immune response toward an anti-inflammatory profile by the increased recruitment of myeloid-derived suppressor cells (MDSCs) that attenuate macrophage proinflammatory activity, leading to chronic infection. A screen of the Nebraska Transposon Mutant Library identified several hits in the ATP synthase operon that elicited a heightened inflammatory response in macrophages and MDSCs, including *atpA*, which encodes the alpha subunit of ATP synthase. An *atpA* transposon mutant ( $\Delta atpA$ ) had altered growth kinetics under both planktonic and biofilm conditions, along with a diffuse biofilm architecture that was permissive for leukocyte infiltration, as observed by confocal laser scanning microscopy. Coculture of MDSCs and macrophages with  $\Delta atpA$  biofilm elicited significant increases in the proinflammatory cytokines interleukin 12p70 (IL-12p70), tumor necrosis factor alpha (TNF- $\alpha$ ), and IL-6. This was attributed to increased leukocyte survival resulting from less toxin and protease production by  $\Delta atpA$  biofilm as determined by liquid chromatography with tandem mass spectrometry (LC-MS/MS). The enhanced inflammatory response elicited by  $\Delta atpA$  biofilm was cell lysis-dependent since it was negated by polyanethole sodium sulfanate treatment or deletion of the major autolysin, Atl. In a mouse model of PJI,  $\Delta atpA$ -infected mice had decreased MDSCs concomitant with increased monocyte/macrophage infiltrates and proinflammatory cytokine production, which resulted in biofilm clearance. These studies identify *S. aureus* ATP synthase as an important factor in influencing the immune response during biofilm-associated infection and bacterial persistence.

**IMPORTANCE** Medical device-associated biofilm infections are a therapeutic challenge based on their antibiotic tolerance and ability to evade immune-mediated clearance. The virulence determinants responsible for bacterial biofilm to induce a maladaptive immune response remain largely unknown. This study identified a critical role for *S. aureus* ATP synthase in influencing the host immune response to biofilm infection. An *S. aureus* ATP synthase alpha subunit mutant ( $\Delta atpA$ ) elicited heightened proinflammatory cytokine production by leukocytes *in vitro* and *in vivo*, which coincided with improved biofilm clearance in a mouse model of prosthetic joint infection. The ability of *S. aureus*  $\Delta atpA$  to augment host proinflammatory responses was cell lysis-dependent, as inhibition of bacterial lysis by polyanethole sodium sulfanate or a  $\Delta atpA\Delta atl$  biofilm did not elicit heightened cytokine production. These studies reveal a critical role for AtpA in shaping the host immune response to *S. aureus* biofilm.

**KEYWORDS** biofilm, cytokines, macrophages, myeloid-derived suppressor cell

**Citation** Bosch ME, Bertrand BP, Heim CE, Alqarzaee AA, Chaudhari SS, Aldrich AL, Fey PD, Thomas VC, Kielian T. 2020. *Staphylococcus aureus* ATP synthase promotes biofilm persistence by influencing innate immunity. mBio 11:e01581-20. <https://doi.org/10.1128/mBio.01581-20>.

**Editor** Victor J. Torres, New York University School of Medicine

**Copyright** © 2020 Bosch et al. This is an open-access article distributed under the terms of the [Creative Commons Attribution 4.0 International license](https://creativecommons.org/licenses/by/4.0/).

Address correspondence to Tammy Kielian, [tkielian@unmc.edu](mailto:tkielian@unmc.edu).

\* Present address: Megan E. Bosch, Washington University School of Medicine, St. Louis, Missouri, USA; Amy L. Aldrich, Moffitt Cancer Center, Tampa, Florida, USA.

**Received** 11 June 2020

**Accepted** 8 August 2020

**Published** 8 September 2020

*Staphylococcus aureus* is an opportunistic pathogen that expresses a wide array of virulence determinants to evade host immune responses (1–4). *S. aureus* can asymptotically colonize several sites of the human body, most often in the anterior nares, where approximately 30% of individuals are persistent *S. aureus* carriers and up to 60% of the population may be intermittent carriers (5, 6). A patient's carrier status is a risk factor for postsurgical *S. aureus* infection (7, 8). This is particularly relevant for arthroplasty procedures, as *S. aureus* is a frequent cause of prosthetic joint infection (PJI) with methicillin-resistant *S. aureus* (MRSA) strains responsible for up to half of these infections (9, 10). As a result, patients who are *S. aureus* carriers are subjected to decolonization protocols prior to arthroplasty as a standard of care at many medical institutions (11, 12). Not only are PJIs often associated with bacteria that harbor genes that encode antibiotic resistance, but they are also typified by biofilm formation, which affords antibiotic tolerance and dampens host proinflammatory immune responses (1, 13, 14).

Biofilms are communities of bacteria encased by a self-produced matrix consisting of proteins, carbohydrates, and extracellular DNA (eDNA) (15, 16). The extracellular matrix provides structure to the biofilm and also allows for nutrient distribution and the exchange of substrates (17). Additionally, there is metabolic diversity within the biofilm, which provides rapid adaptation to stressors and antibiotic tolerance (16). Our laboratory has previously shown in a mouse model of PJI that *S. aureus* biofilm can actively suppress proinflammatory responses by the preferential recruitment of myeloid-derived suppressor cells (MDSCs) and anti-inflammatory monocytes/macrophages (M $\Phi$ s) to the site of infection (14, 18). These MDSCs produce interleukin 10 (IL-10) to create an immunosuppressive environment that allows for biofilm persistence (19, 20). Importantly, MDSC infiltrates are also more pronounced in tissues from patients with PJI than with aseptic loosening, reinforcing the findings in the mouse PJI model (21, 22).

A screen of the Nebraska Transposon Mutant Library (NTML) (23) was conducted to identify mutations that elicited a heightened proinflammatory response from M $\Phi$ s and MDSCs during coculture with mature *S. aureus* biofilm. Significant hits occurred in genes within the ATP synthase operon, specifically in *atpA*, *atpD*, and *atpG*. These genes encode the alpha, beta, and gamma subunits of the ATP synthase catalytic core, respectively. ATP synthase is a central metabolic enzyme that is driven by the proton motive force generated by the respiratory chain, and it functions to synthesize ATP (24, 25). With regard to *S. aureus*, a recent study identified that *atpG* was required for virulence in a mouse model of skin and soft tissue infection (SSTI) (26). This was attributed, in part, to a failure in intracellular acidification, which is required for the optimal activity of fermentative enzymes that generate energy in the face of respiration defects (26). However, the role of *S. aureus* ATP synthase in influencing biofilm development and subsequent effects on host immunity has not yet been explored. In this report, we show that *atpA* was essential for biofilm persistence in a mouse model of PJI. Disruption of *atpA* reduced toxin and protease production, which resulted in a heightened proinflammatory response due to enhanced leukocyte survival.

## RESULTS

**ATP synthase plays a critical role in dictating biofilm growth and structure.** To characterize the role of *S. aureus* ATP synthase in influencing MDSC and M $\Phi$  activation, we focused on *atpA* since this gene is upstream of *atpD* and *atpG* in the operon and, as such, was also inactivated in the NTML *atpA* mutant. These subunits compose the catalytic core of ATP synthase; therefore, disruption of these genes renders the enzyme nonfunctional. Bacterial ATP synthase is critical for energy production, homeostasis, and maintaining the proton motive force (24). Therefore, we first characterized the growth kinetics of  $\Delta$ *atpA*, which was assessed in tryptic soy broth (TSB) and RPMI-1640 with 1% Casamino Acids (CAA) under both planktonic and biofilm growth conditions. RPMI-1640 is a standard base medium for eukaryotic cells and was utilized throughout this study for biofilm-leukocyte coculture experiments since it better models the

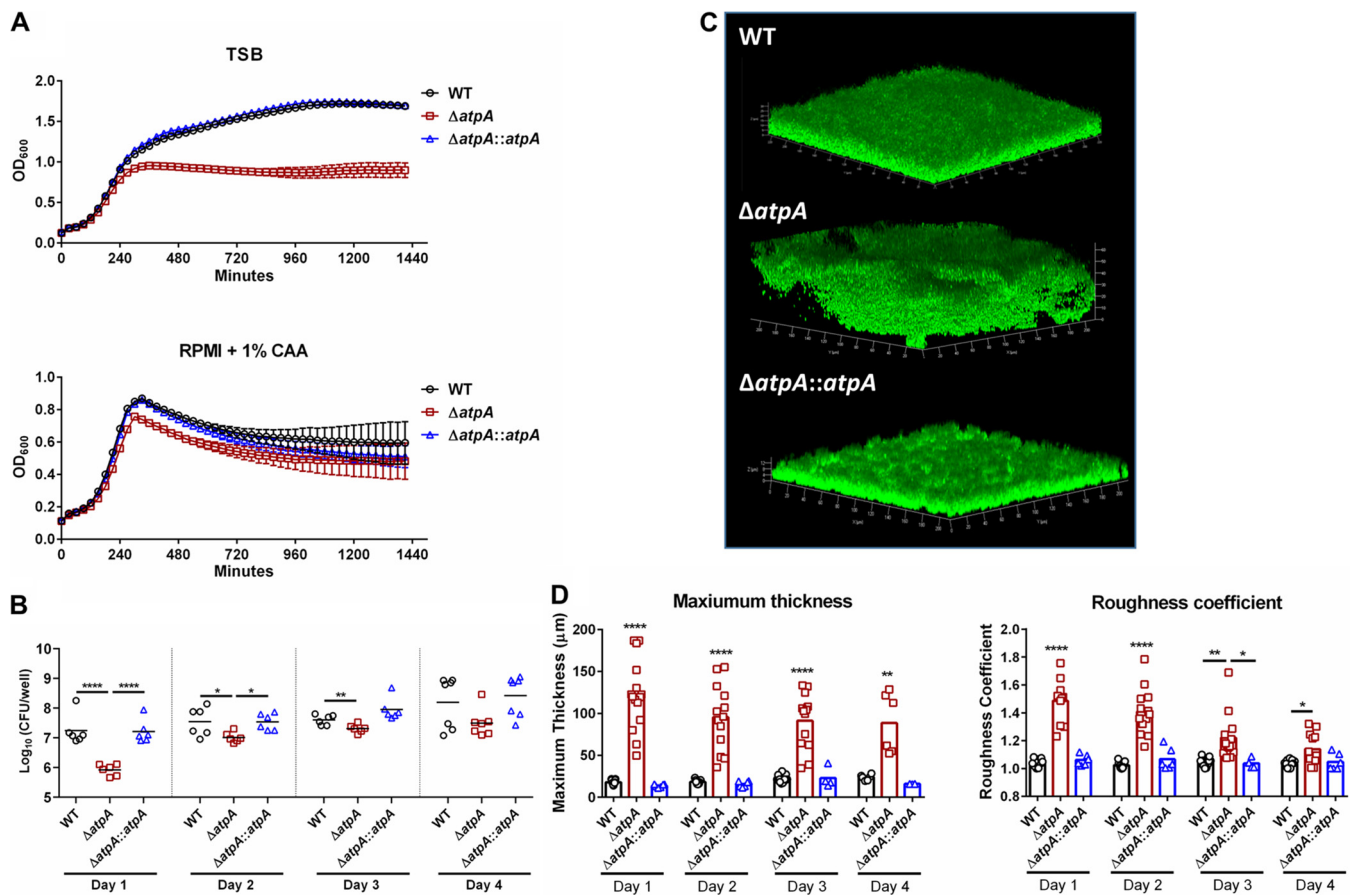


**FIG 1** *S. aureus*  $\Delta atpA$  biofilm displays early growth defects and altered structure. (A and B) The growth of *S. aureus* WT,  $\Delta atpA$ , and  $\Delta atpA::atpA$  was characterized by OD<sub>600</sub> in tryptic soy broth (TSB) or RPMI-1640 supplemented with 1% Casamino Acids (CAA; mean  $\pm$  SD of one representative experiment;  $n = 6$  biological replicates) (A) and CFU of *in vitro* biofilm at various stages of development (mean combined from 2 independent experiments;  $n = 6$  biological replicates) (B). (C) Representative three-dimensional (3D) images of 4-day-old biofilm acquired using confocal laser scanning microscopy. (D) Maximum thickness and roughness coefficient measurements were calculated by Comstat 2 analysis (mean combined from 1 to 4 independent experiments;  $n = 3$  to 15 biological replicates). Significant differences are denoted by asterisks (\*,  $P < 0.05$ , \*\*,  $P < 0.01$ , and \*\*\*\*,  $P < 0.0001$ ; one-way ANOVA with Tukey's multiple-comparison test).

mammalian tissue milieu compared to TSB.  $\Delta atpA$  displayed a postexponential-phase growth defect in both medium formulations compared to wild type (WT) (Fig. 1A). Biofilm burden was reduced in  $\Delta atpA$  during the first 3 days of growth but then reached titers similar to WT biofilm (Fig. 1B). Biofilm architecture was notably different in  $\Delta atpA$ , with an increased maximum thickness and roughness coefficient compared to WT (Fig. 1C to D). All the  $\Delta atpA$  phenotypes were complementable (Fig. 1).

***S. aureus* ATP synthase attenuates MDSC and M $\Phi$  inflammatory responses to biofilm.** Previous studies from our laboratory have demonstrated that *S. aureus* biofilm skews leukocytes to an anti-inflammatory state, which promotes bacterial persistence (18, 19, 27). To determine if *S. aureus* ATP synthase-dependent pathways play a role in this process, primary bone marrow-derived MDSCs and M $\Phi$ s were cocultured with  $\Delta atpA$  biofilm to quantify cytokine production. MDSCs and M $\Phi$ s exposed to  $\Delta atpA$  biofilm produced significantly higher levels of the proinflammatory cytokines IL-12p70, tumor necrosis factor alpha (TNF- $\alpha$ ), and IL-6 than WT biofilm (Fig. 2A). Although the anti-inflammatory cytokine IL-10 was also significantly elevated in response to  $\Delta atpA$  (Fig. 2A), collectively, the increases in IL-12p70, TNF- $\alpha$ , and IL-6 suggest a proinflammatory bias in response to  $\Delta atpA$  biofilm. These findings were replicated in human monocyte-derived M $\Phi$ s, where TNF- $\alpha$ , IL-6, and IL-8 production was significantly enhanced in response to  $\Delta atpA$  compared to WT biofilm, whereas IL-10 release was minimal and not affected (Fig. 2B). The increased cytokine production elicited by  $\Delta atpA$

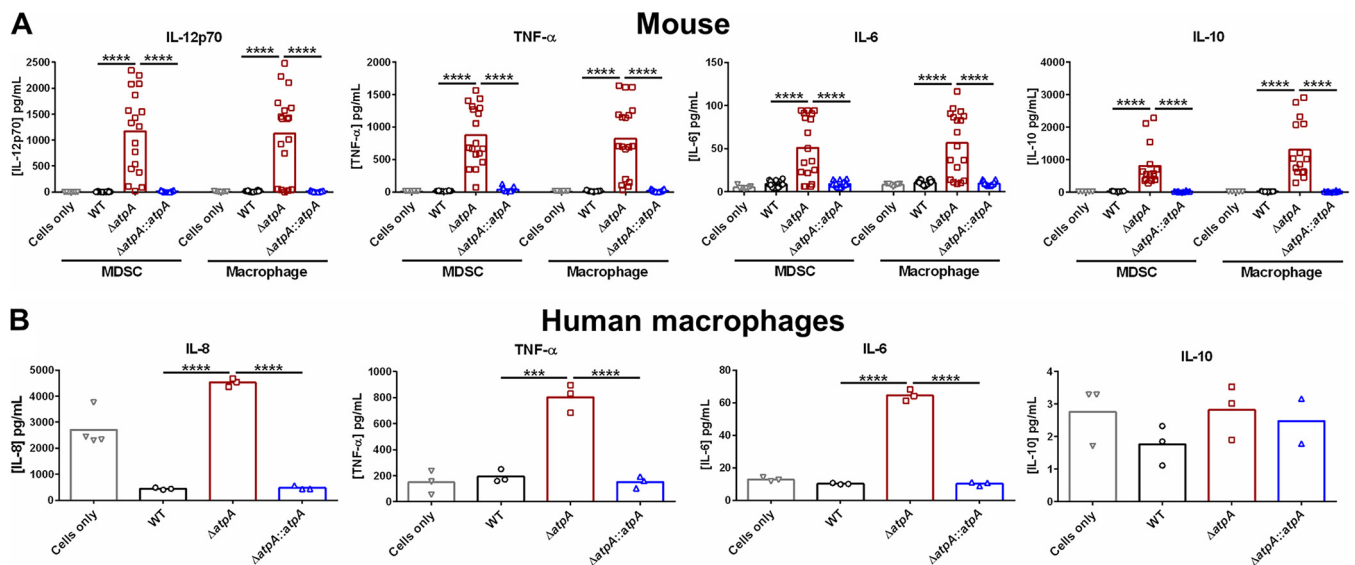


**FIG 2** *AtpA* is critical for attenuating leukocyte cytokine production in response to *S. aureus* biofilm. *S. aureus* 4-day-old biofilms were cocultured with  $5 \times 10^4$  mouse bone marrow-derived MDSCs or macrophages (A) or human monocyte-derived macrophages (B) for 2 h, whereupon cytokine production was quantified using a mouse or human cytometric bead array inflammation kit. Results represent the mean combined from 4 independent experiments ( $n = 7$  to 21 biological replicates) (A) and mean of 1 experiment ( $n = 3$  biological replicates) (B) repeated with monocytes from 3 different donors. Significant differences are denoted by asterisks (\*\*\*,  $P < 0.001$ , and \*\*\*\*,  $P < 0.0001$ ; one-way ANOVA with Tukey's multiple-comparison test).

biofilm in mouse and human leukocytes was complementable (Fig. 2). Heightened proinflammatory cytokine release was also elicited by  $\Delta atpD$  and  $\Delta atpG$  biofilm (Fig. S1), highlighting the importance of ATP synthase in influencing leukocyte activation. Additionally,  $\Delta atpA$  was more susceptible to killing by mouse M $\Phi$ s (Fig. S2), demonstrating that functional ATP synthase renders *S. aureus* more resistant to M $\Phi$  bactericidal activity.

We next determined if the diffuse structure of  $\Delta atpA$  biofilm (Fig. 1C and D) altered M $\Phi$  interactions since previous studies demonstrated that M $\Phi$ s are unable to invade a WT *S. aureus* biofilm (28, 29).  $\Delta atpA$  biofilm had more M $\Phi$ s contacting the biofilm surface as visualized by confocal laser scanning microscopy, whereas M $\Phi$ s were excluded from WT biofilm (Fig. 3A). The diffuse structure of  $\Delta atpA$  biofilm could make pathogen-associated molecular patterns (PAMPs), such as lipoteichoic acid (LTA), peptidoglycan (PGN), and eDNA, more accessible to invading leukocytes to account for their heightened cytokine production. This possibility was further supported by the finding that eDNA concentrations were significantly increased in  $\Delta atpA$  biofilm (Fig. 3B). *S. aureus* LTA and PGN are recognized by Toll-like receptor 2 (TLR2), and eDNA engages TLR9, with both TLRs signaling through myeloid differentiation factor 88 (MyD88) (30, 31). To assess the role of PAMPs in potentiating the inflammatory response to  $\Delta atpA$  biofilm, cocultures were performed with TLR2<sup>-/-</sup> or MyD88<sup>-/-</sup> MDSCs and M $\Phi$ s. The response to  $\Delta atpA$  biofilm was equivalent for WT, TLR2<sup>-/-</sup>, and MyD88<sup>-/-</sup> MDSCs and M $\Phi$ s, indicating that the heightened cytokine response to  $\Delta atpA$  biofilm was MyD88- and TLR2-independent (Fig. 4). MyD88<sup>-/-</sup> MDSCs and M $\Phi$ s were unresponsive to TLR2 (Pam3CSK4 and PGN) and TLR9 (CpG DNA) agonists, confirming defects in TLR signaling (Fig. S3). However, leukocyte viability during the biofilm coculture period revealed increased MDSC and M $\Phi$  survival with  $\Delta atpA$  compared to WT biofilm (Fig. 5). Therefore, enhanced cytokine production by leukocytes cocultured with  $\Delta atpA$  biofilm likely results, in part, from an increased number of viable cells being able to sustain cytokine production and not from improved recognition of biofilm antigens.

To identify proteins that may contribute to the increased survival of MDSCs and M $\Phi$ s in response to  $\Delta atpA$  biofilm, liquid chromatography with tandem mass spectrometry (LC-MS/MS) was performed. This analysis revealed a significant reduction in many virulence factors and toxins in  $\Delta atpA$  biofilm supernatants, including serine

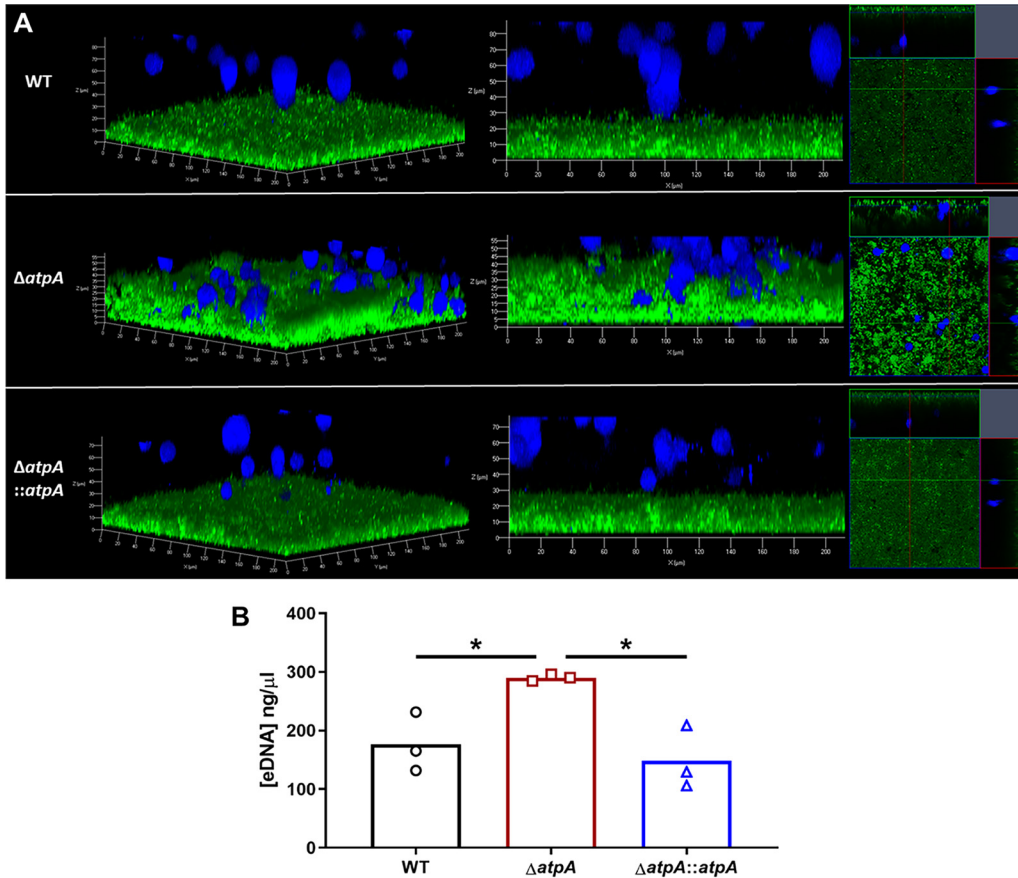


**FIG 3** *S. aureus* AtpA prevents macrophage biofilm invasion and regulates eDNA release. (A) Bone marrow-derived macrophages were stained with CellTracker deep red (pseudocolored blue) and cocultured for 2 h with 6-day-old *S. aureus* biofilm transduced with a GFP reporter plasmid and imaged by confocal laser scanning microscopy. Representative 3D (left) and side view (middle) z-stack images, as well as orthogonal views (right), are shown from two independent experiments, each with one biological replicate and 5 to 6 images per replicate. (B) *S. aureus* biofilms were grown in 6-well plates, whereupon eDNA was quantified at day 6 by quantitative PCR. Results represent the mean from one experiment ( $n = 3$  biological replicates). Significant differences are denoted by asterisks (\*,  $P < 0.05$ ; one-way ANOVA with Tukey's multiple-comparison test).

proteases,  $\alpha$ -hemolysin, and leukocidin-like proteins that are known to induce leukocyte death (2) (Table 1; Fig. S4; Data Set S1), supporting the observations of more viable MDSCs and MΦs in  $\Delta atpA$  biofilm cocultures and the lack of hemolysis by  $\Delta atpA$  on blood agar (data not shown). LC-MS/MS also confirmed decreased levels of ATP synthase subunits as well as select metabolic enzymes in  $\Delta atpA$  biofilm extracts (Table 2; Fig. S4B; Data Set S2).

***S. aureus* ATP synthase contributes to biofilm persistence during orthopedic implant infection.** To elucidate the role of *S. aureus* ATP synthase during biofilm infection, a mouse model of PJI was utilized. To ensure an equal growth phase of WT and  $\Delta atpA$  prior to *in vivo* inoculation, bacteria were collected in exponential phase at an optical density at 600 nm ( $OD_{600}$ ) of 0.25 (Fig. S5). A similar heightened inflammatory profile was observed during PJI with  $\Delta atpA$  as was seen *in vitro*, with significantly higher levels of IL-6, TNF- $\alpha$ , IFN- $\gamma$ , granulocyte colony-stimulating factor (G-CSF), granulocyte-macrophage colony-stimulating factor (GM-CSF), monocyte chemoattractant protein 5 (CCL5), and interferon-inducible protein 10 kDa (CXCL10) expression, primarily at day 7 postinfection (Fig. 6). Although IL-10 levels were also significantly elevated in response to  $\Delta atpA$  (Fig. 6D), the totality of the data suggest a proinflammatory bias in response to  $\Delta atpA$  biofilm. Additional proinflammatory mediators were also elevated in  $\Delta atpA$ -infected mice, although these did not reach statistical significance (Fig. S6). The enhanced proinflammatory response in  $\Delta atpA$ -infected mice coincided with reduced

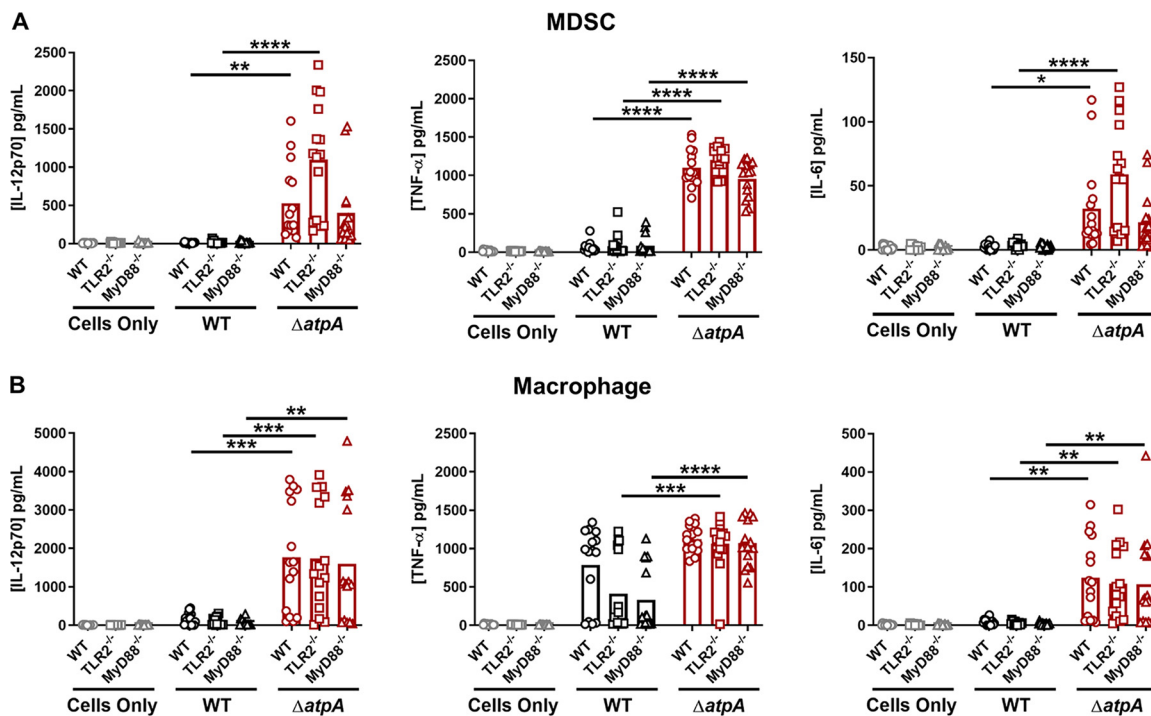


**FIG 4** Enhanced proinflammatory mediator production elicited by *S. aureus*  $\Delta atpA$  biofilm is TLR2- and MyD88-independent. WT, MyD88<sup>-/-</sup>, and TLR2<sup>-/-</sup> bone marrow-derived MDSCs (A) and macrophages (B) were cocultured with 4-day-old WT or  $\Delta atpA$  biofilm for 2 h, whereupon supernatants were analyzed using a mouse cytometric bead array inflammation kit. Results represent the mean combined from 3 independent experiments ( $n = 15$  biological replicates). Significant differences are denoted by asterisks (\*,  $P < 0.05$ , \*\*,  $P < 0.01$ , \*\*\*,  $P < 0.001$ , and \*\*\*\*,  $P < 0.0001$ , one-way ANOVA with Tukey's multiple-comparison test).

bacterial burden in the tissue, knee joint, and femur (Fig. 7A), concomitant with decreased MDSC and increased monocyte and M $\Phi$  infiltrates in the infected tissue (Fig. 7B) that was completable (Fig. 7C). Furthermore, functional ATP synthase was necessary for establishing persistent PJI, as  $\Delta atpA$ -infected mice had no detectable bacteria in implant-associated tissues at 3 months postinfection (Fig. S7).

#### Inhibiting cell lysis in $\Delta atpA$ attenuates leukocyte proinflammatory responses.

We next investigated potential mechanisms for the unique structure of  $\Delta atpA$  biofilm that may account for its ability to enhance leukocyte cytokine release. A major component of the extracellular polymeric substance (EPS) of biofilm is eDNA, which is released by the lysis of a subset of bacterial cells within the biofilm (32). Since eDNA levels were significantly increased in  $\Delta atpA$  biofilm (Fig. 3B), we examined whether inhibiting biofilm lysis with polyanethole sodium sulfanate (PAS), which blocks the major *S. aureus* autolysin Atl (33), would reverse the heightened inflammatory response elicited by  $\Delta atpA$ . PAS treatment of  $\Delta atpA$  biofilm significantly reduced eDNA levels (Fig. 8A), resulting in a more compact structure (Fig. 8B and C). PAS had little effect on WT biofilm, both in terms of morphology and eDNA release (Fig. 8). Treatment with DNase partially restored  $\Delta atpA$  biofilm structure (Fig. 8B), suggesting the involvement of other cell lysis-dependent factors. Overall, these data suggest that enhanced eDNA release partially contributes to the altered structure of  $\Delta atpA$  biofilm, which can be reversed by inhibiting cell lysis. PAS treatment also diminished the enhanced proinflammatory response of MDSCs and M $\Phi$ s to  $\Delta atpA$  biofilm (Fig. 9). Even though DNase treatment partially restored biofilm structure, it did not attenuate cytokine production elicited by  $\Delta atpA$  biofilm (Fig. 9), revealing that leukocyte activation is driven by cell lysis-dependent factors other than eDNA in agreement with the findings with MyD88<sup>-/-</sup> leukocytes (Fig. 4). PAS treatment significantly reduced macrophage viability following coculture with  $\Delta atpA$  biofilm (Fig. 9D), in agreement with

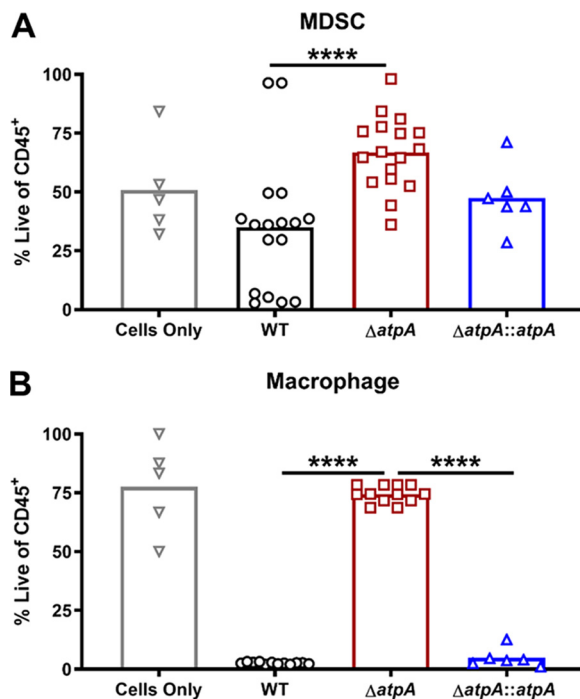


**FIG 5** *S. aureus* AtpA dictates leukocyte survival during biofilm coculture. Bone marrow-derived MDSCs (A) or macrophages (B) were cocultured with 4-day-old biofilm for 2 h, whereupon cell viability was accessed by flow cytometry using a live/dead stain. Results are presented as the percentage of live CD45-positive (CD45<sup>+</sup>) leukocytes and represent the mean combined from 3 independent experiments ( $n = 5$  to 17 biological replicates). Significant differences are denoted by asterisks (\*\*\*\*,  $P < 0.0001$ ; one-way ANOVA with Tukey's multiple-comparison test).

its ability to diminish cytokine production to levels observed with WT biofilm (Fig. 9B). A similar trend was observed with MDSCs, although this did not reach statistical significance (Fig. 9C). Macrophage viability was also reduced during coculture with DNase-treated  $\Delta atpA$  biofilm, but this was less dramatic than PAS (Fig. 9D).

**Deletion of the major *S. aureus* autolysin Atl reverses heightened proinflammatory cytokine release from leukocytes in response to  $\Delta atpA$  biofilm.** A main target of PAS in staphylococci is autolysins (33), and the major *S. aureus* autolysin, Atl, plays a role in cell wall turnover, division, and biofilm formation (34, 35). Since PAS treatment attenuated leukocyte proinflammatory cytokine production in response to  $\Delta atpA$  biofilm, we constructed a double-mutant strain ( $\Delta atpA \Delta atl$ ) to assess the role of Atl-mediated cell lysis in  $\Delta atpA$  biofilm. As expected, both *atpA* and *atl* were critical for *S. aureus* growth in broth and biofilm culture, and the  $\Delta atpA \Delta atl$  strain exhibited attenuated growth under both conditions (Fig. 10A and B). However, the diffuse biofilm structure of  $\Delta atpA$  was reversed in  $\Delta atpA \Delta atl$  with a significant reduction in the maximum thickness and roughness coefficients (Fig. 10C and D). Atl-mediated lysis also contributed to the enhanced cytokine production by MDSCs and M $\Phi$ s in response to  $\Delta atpA$  biofilm since this was significantly reduced in  $\Delta atpA \Delta atl$  (Fig. 11). Taken together, our findings demonstrate that the increased inflammatory properties of MDSCs and M $\Phi$ s cocultured with  $\Delta atpA$  biofilm is a lysis-dependent phenotype since the chemical inhibition of cell lysis or Atl deletion dampens leukocyte cytokine production.

## DISCUSSION

In the present study, a screen of the NTML identified a role for *S. aureus* ATP synthase in attenuating MDSC and M $\Phi$  cytokine production, and *S. aureus*  $\Delta atpA$  was cleared in a mouse model of PJI, demonstrating the importance of ATP synthase in

**TABLE 1** Virulence factors are significantly reduced in supernatants from  $\Delta atpA$  biofilm

Protein	Gene	Log <sub>2</sub> difference ( $\Delta atpA$ /WT) <sup>a</sup>
Serine protease SplC	<i>splC</i>	-4.34
Serine protease SplE	<i>splE</i>	-3.94
Serine protease SplF	<i>splF</i>	-3.89
Serine protease SplB	<i>splB</i>	-3.85
Uncharacterized leukocidin-like protein 2	SAB1876c	-2.63
Lipase 1	<i>lip1</i>	-2.50
Zinc metalloproteinase aureolysin	<i>aur</i>	-2.45
Alpha-hemolysin	<i>hly</i>	-2.38
Lipase 2	<i>lip2</i>	-2.36
Lysozyme-like protein 7	<i>lys-7</i>	-2.02
UPF0173 metal-dependent hydrolase SAUSA300_1653	SAUSA300_1653	-1.92
1-phosphatidylinositol phosphodiesterase	<i>plc</i>	-1.75
Uncharacterized leukocidin-like protein 1	SAOUHSC_02241	-1.53
Glutamyl-tRNA(Gln) amidotransferase subunit A	<i>gatA</i>	-1.43
Uncharacterized lipoprotein SAOUHSC_02650	SAOUHSC_02650	-1.38
Staphopain A	<i>sspP</i>	-1.37
Aspartate carbamoyltransferase	<i>pyrB</i>	-1.37
50S ribosomal protein L16	<i>rplP</i>	-1.36
Staphylokinase	<i>sak</i>	-1.31
Elastin-binding protein EbpS	<i>ebpS</i>	-1.30
33-kDa chaperonin	<i>hslO</i>	-1.20
50S ribosomal protein L17	<i>rplQ</i>	-1.10
Clumping factor A	<i>clfA</i>	-1.10
Serine protease SplA	<i>splA</i>	-1.03

<sup>a</sup>All proteins were significantly different;  $P < 0.05$ .

biofilm persistence. This report provides a link between bacterial ATP synthase activity and host immunity during biofilm development, which is largely influenced by increased bacterial cell lysis.

Previous studies have shown that the inactivation of *S. aureus* ATP synthase leads to increased susceptibility to polymyxins, gentamicin, and nitric oxide (26, 36, 37). ATP synthase is the primary energy generator for cellular respiration, so it was not unexpected that *atpA* disruption affected *S. aureus* growth in both planktonic and biofilm conditions. Interestingly,  $\Delta atpA$  biofilm elicited heightened proinflammatory cytokine production in mouse MDSCs and MΦs, and similar results were obtained with human monocyte-derived MΦs, demonstrating the translational relevance of these findings.

**TABLE 2** Metabolic protein expression is reduced in  $\Delta atpA$  biofilm extracts

Protein	Gene	Log <sub>2</sub> difference ( $\Delta atpA$ /WT) <sup>a</sup>
ATP synthase subunit alpha	<i>atpA</i>	-5.08
ATP synthase gamma chain	<i>atpG</i>	-3.71
ATP synthase subunit beta	<i>atpD</i>	-3.39
ATP synthase subunit b	<i>atpF</i>	-3.35
Arginine deiminase	<i>arcA</i>	-1.74
Low-molecular-weight protein-tyrosine-phosphatase	<i>ptpA</i>	-1.68
Threonine-tRNA ligase	<i>thrS</i>	-1.59
Ornithine carbamoyltransferase	<i>argF</i>	-1.47
Carbamate kinase 2	<i>arcC2</i>	-1.28
Alanine dehydrogenase 1	<i>ald1</i>	-1.27
Dihydroorotase	<i>pyrC</i>	-1.26
L-Threonine dehydratase catabolic TdcB	<i>tdcB</i>	-1.24
Alcohol dehydrogenase	<i>adh</i>	-1.23
Carbamate kinase 1	<i>arcC1</i>	-1.19
ATP synthase subunit delta	<i>atpH</i>	-1.13
DNA-binding protein HU	<i>hup</i>	-1.13
Argininosuccinate synthase	<i>argG</i>	-1.04
Formimidoylglutamate	<i>hutG</i>	-1.03
Clumping factor A	<i>clfA</i>	-1.02

<sup>a</sup>All proteins were significantly different;  $P < 0.05$ .



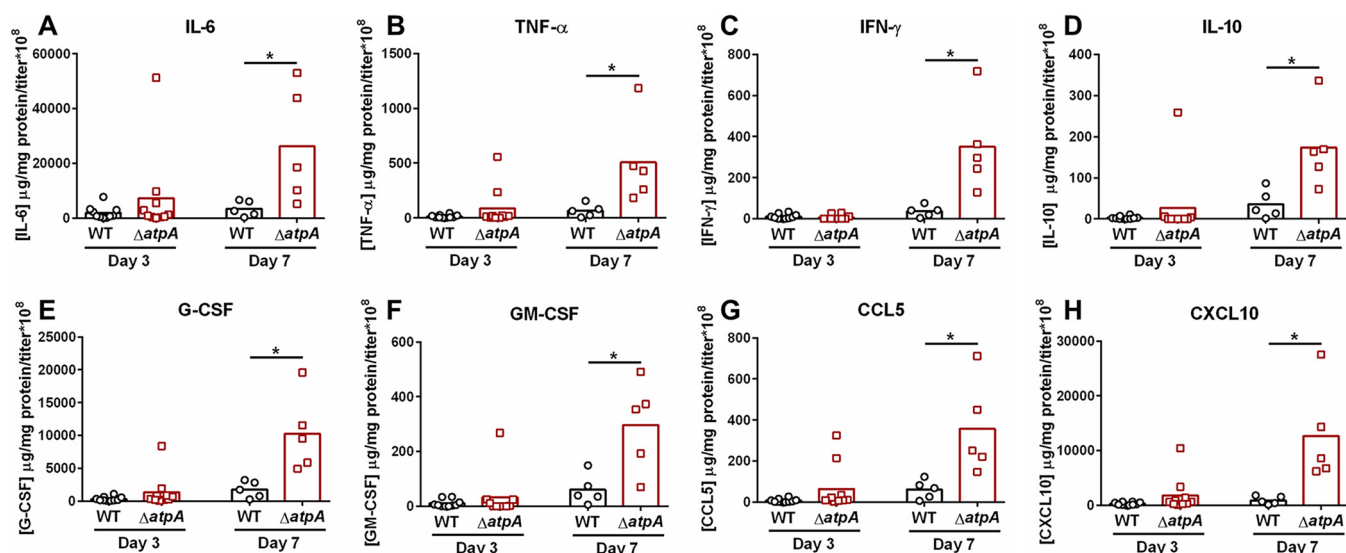


**FIG 6** *S. aureus* AtpA attenuates inflammatory mediator production during prosthetic joint infection (PJI). C57BL/6NCR1 mice were infected with  $10^3$  CFU of *S. aureus* WT or  $\Delta atpA$  using a model of PJI. Implant-associated tissue was collected at days 3 or 7 postinfection, and inflammatory mediators quantified using a multianalyte bead array. IL-6 (A), TNF- $\alpha$  (B), IFN- $\gamma$  (interferon-gamma) (C), IL-10 (D), G-CSF (granulocyte colony-stimulating factor) (E), GM-CSF (granulocyte-macrophage colony-stimulating factor) (F), CCL5 (regulated upon activation T cell expressed and secreted; RANTES) (G), and CXCL10 (interferon-inducible protein 10 kDa) (H) concentrations were normalized to the protein concentration per sample and bacterial titer of each mouse to correct for differences in infectious burden between WT and  $\Delta atpA$ . Results from day 3 represent the mean combined from 2 independent experiments ( $n = 10$  mice/group) and day 7 from one experiment ( $n = 5$  mice/group). Significant differences are denoted by asterisks (\*,  $P < 0.05$ ; Student's *t* test with Holm-Sidak correction).

The increase in cytokine production likely resulted from improved leukocyte viability based on the reductions in toxin and protease production by  $\Delta atpA$  biofilm. Of note, a prior screen of the NTML identified *atpA* as important for attenuating macrophage proinflammatory cytokine production in response to planktonic *S. aureus* (38), revealing the broader implications for bacterial ATP synthase-dependent mechanisms in dictating leukocyte activation.

The essential role of *S. aureus* ATP synthase in influencing the host inflammatory response during biofilm formation *in vivo* was demonstrated by the finding that  $\Delta atpA$  was cleared in a mouse PJI model at 3 months postinfection. However, it is important to emphasize the differential involvement of *S. aureus* ATP synthase during biofilm versus nonbiofilm infections. For example, a recent study by Grosser et al. in a mouse SSTI model demonstrated that *S. aureus*  $\Delta atpG$  was cleared within 3 days (26), whereas in the current study,  $\Delta atpA$  was still detected at day 28 postinfection in a mouse PJI biofilm model. This highlights the distinctions in *S. aureus* persistence between biofilm versus acute tissue infection, and the metabolic state of bacteria in each setting may explain the differential survival of *S. aureus* ATP synthase mutants.

*S. aureus* biofilms exhibit metabolic heterogeneity, with a subpopulation of metabolically dormant organisms (39, 40). Therefore, it is conceivable that this population of cells is more recalcitrant to the loss of *S. aureus* ATP synthase, enabling their increased survival in the host. This is supported by a recent study demonstrating that ATP depletion is responsible for promoting antibiotic-tolerant persister cells in *S. aureus* (41). In contrast, *S. aureus* is metabolically active during acute tissue infection, which may explain why bacteria are more sensitive to the loss of respiratory capacity and rapidly cleared. Indeed, the reduced fitness of  $\Delta atpG$  was attributed, in part, to a failure in intracellular acidification, which is required for the optimal activity of fermentative enzymes that generate energy in the face of respiration defects (26). A critical role for *S. aureus* *atpA* in attenuating the host immune response *in vivo* was demonstrated by the finding that  $\Delta atpA$  elicited heightened proinflammatory mediator production in a mouse model of *S. aureus* PJI. This coincided with a significant reduction in MDSCs concomitant with increased monocyte and  $M\Phi$  recruitment, a relationship that our prior studies have established coincides with biofilm clearance (18, 20, 22, 27, 42).

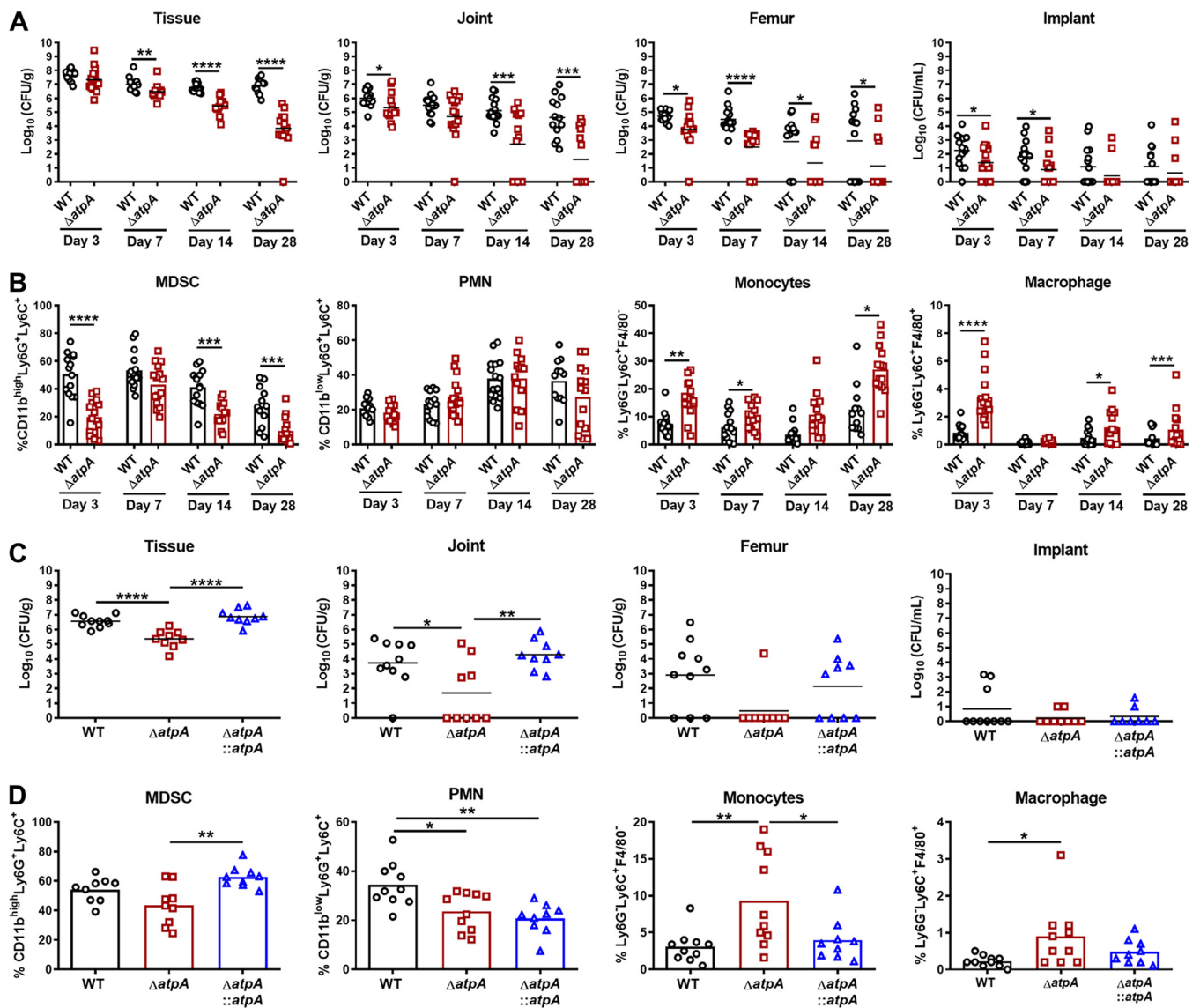


**FIG 7** *S. aureus* AtpA is critical for regulating leukocyte influx and biofilm persistence. (A) C57BL/6NCR1 mice were infected with  $10^3$  CFU of *S. aureus* WT or  $\Delta atpA$  using a model of prosthetic joint infection. Animals were sacrificed at the indicated intervals, whereupon bacterial burden in the implant-associated tissue, joint, femur, and implant was quantified with results expressed as  $\log_{10}$ -transformed values from 3 independent experiments ( $n = 13$  to 16 mice/group). (B) Flow cytometry was performed on implant-associated tissue to quantify infiltrating leukocyte populations. (C) Bacterial burden and (D) leukocyte influx are shown for complementation studies at day 14 postinfection combined from 2 independent experiments ( $n = 9$  to 10 mice/group). Significant differences are denoted by asterisks (\*,  $P < 0.05$ , \*\*,  $P < 0.01$ , \*\*\*,  $P < 0.001$ , and \*\*\*\*,  $P < 0.0001$ ; one-way ANOVA with Tukey's multiple-comparison test).

We hypothesized that the diffuse structure of  $\Delta atpA$  biofilm might enable better recognition of *S. aureus* PAMPs leading to increased cytokine production, which was suggested by elevated eDNA levels in  $\Delta atpA$  biofilm. However, this seems unlikely, since cytokine levels were equivalent in MyD88<sup>-/-</sup> and WT leukocytes following coculture with  $\Delta atpA$  biofilm, although a role for MyD88-independent pathways cannot be disregarded (i.e., nucleotide-binding and oligomerization domain [NOD] receptors). In terms of TLR9 involvement, this was not unexpected since TLR9 is an endosomal receptor (43) and MΦs fail to phagocytose *S. aureus* biofilm (42), which would prevent eDNA from triggering TLR9 intracellularly. Furthermore, treatment of  $\Delta atpA$  biofilm with DNase did not attenuate enhanced cytokine release by MDSCs or MΦs.

A prior study from our laboratory revealed a critical role for bacterial lysis in blocking MΦ phagocytosis in response to *S. aureus* biofilm (42). In the current report, we found that inhibiting lysis of *S. aureus*  $\Delta atpA$  using two independent approaches, namely, PAS

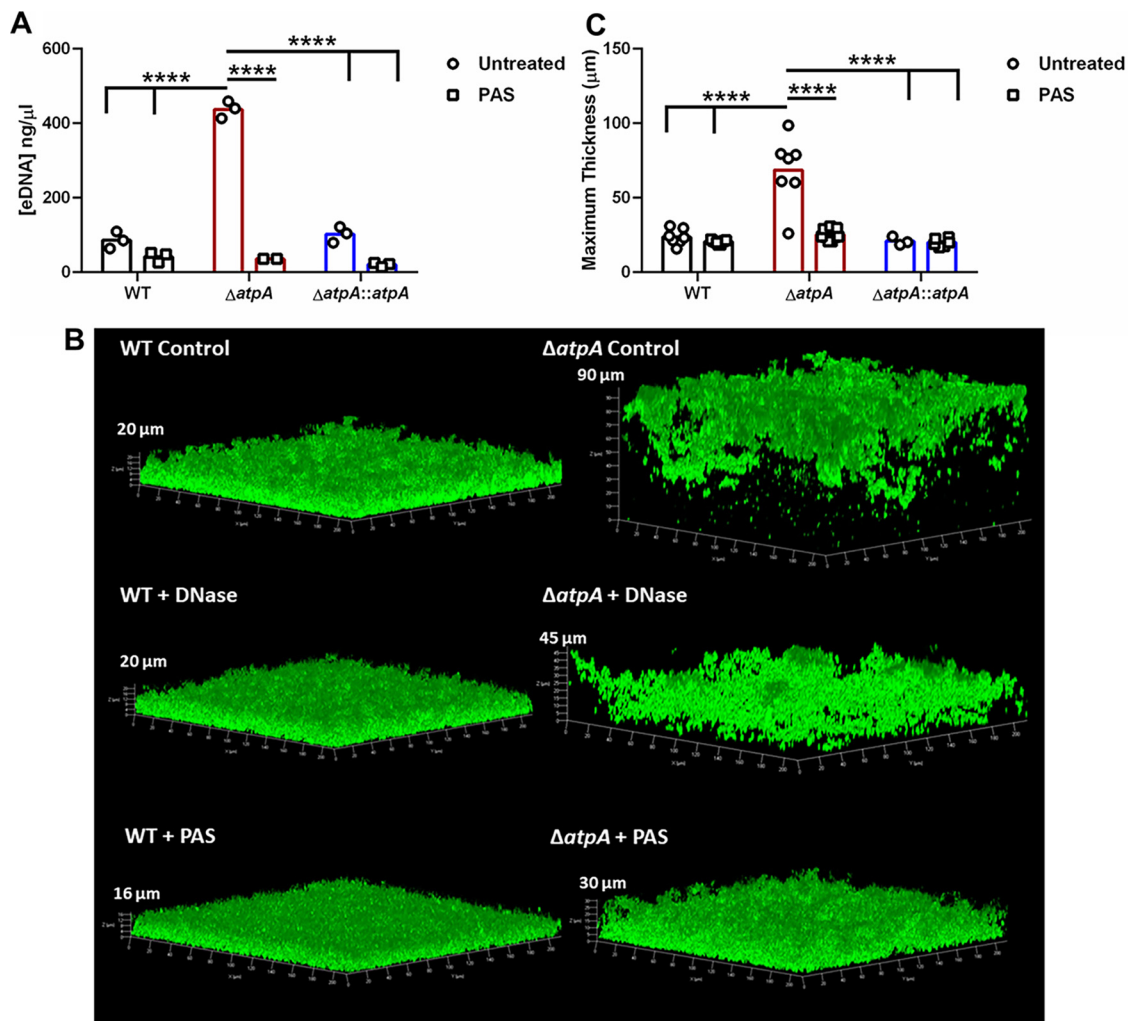


**FIG 8** Inhibiting bacterial lysis negates the aberrant morphology and eDNA levels of *S. aureus*  $\Delta atpA$  biofilm. (A) Biofilms were grown in 6-well plates in the presence of PAS (10  $\mu\text{g}/\text{ml}$ ), and eDNA concentrations were quantified at day 3 ( $n = 2$  to 3 biological replicates). (B) GFP-expressing WT or  $\Delta atpA$  were grown in 8-well chamber slides and treated with DNase (100 U/ml) or PAS (10  $\mu\text{g}/\text{ml}$ ) at the time of biofilm inoculation and throughout the 4-day maturation period, whereupon images were acquired by confocal laser scanning microscopy. (C) Maximum thickness of biofilms was calculated using Comstat 2 combined from 1 to 3 independent experiments ( $n = 3$  to 9 biological replicates). Significant differences are denoted by asterisks (\*\*\*\*,  $P < 0.0001$ ; two-way ANOVA with Tukey's multiple-comparison test).

treatment or a  $\Delta atpA\Delta atI$  strain, negated the enhanced proinflammatory cytokine response by MDSCs and M $\Phi$ s. This finding suggests that factors released following  $\Delta atpA$  biofilm lysis are responsible for promoting leukocyte proinflammatory activity. Additionally, LC-MS/MS analysis revealed a significant reduction in numerous toxins and proteases in  $\Delta atpA$  compared to WT biofilm. Among the proteins that were significantly reduced in  $\Delta atpA$  biofilm were serine proteases of the Spl family (SplB, SplC, SplE, and SplF) and aureolysin, in addition to several toxins, such as Hla and leukocidin-like proteins. It is well established that Hla and leukocidins induce leukocyte lysis by binding to specific immune receptors (2, 44–46), which suggested that the reduction in these virulence factors in  $\Delta atpA$  biofilm may be responsible for the increased viability of MDSCs and M $\Phi$ s. Indeed, this was observed and suggested that the increase in proinflammatory cytokines in response to  $\Delta atpA$  biofilm resulted from a larger number of viable leukocytes that continued to produce cytokines. This highlights the critical role of toxins targeting leukocyte survival, in agreement with earlier reports (47). Our recent study identified many of the same proteins to be responsible for inhibiting M $\Phi$  phagocytosis in response to *S. aureus* biofilm (42).

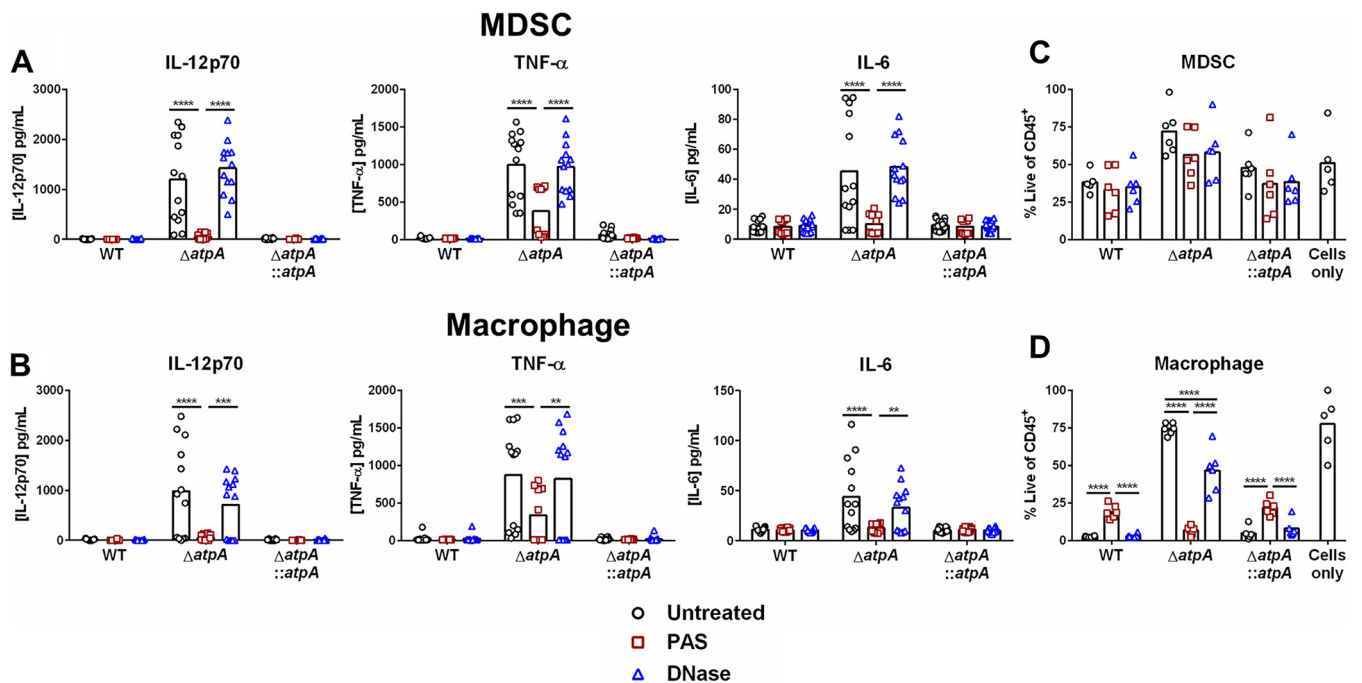


**FIG 9** AtpA-dependent inhibition of leukocyte cytokine production is cell lysis-dependent. Bone marrow-derived MDSCs (A) or macrophages (B) were cocultured for 2 h with biofilm treated with DNase (100 U/ml) or PAS (10  $\mu$ g/ml), whereupon supernatants were analyzed using a mouse cytometric bead array inflammation kit (results represent the mean combined from 3 independent experiments;  $n = 13$  to 16 biological replicates). Viability of MDSCs (C) and macrophages (D) following PAS or DNase treatment with results presented as the percentage of live CD45<sup>+</sup> leukocytes ( $n = 5$  to 6 biological replicates from 2 independent experiments). Significant differences are denoted by asterisks (\*\*,  $P < 0.01$ , \*\*\*,  $P < 0.001$ , and \*\*\*\*,  $P < 0.0001$ ; two-way ANOVA with Tukey's multiple-comparison test).

It remains unclear what combination of factors is responsible for inhibiting leukocyte proinflammatory responses to WT biofilm as demonstrated in this study. The metabolic deficit following the loss of ATP synthase in *S. aureus* likely impinges on multiple pathways, making the ability to pinpoint the phenotypes to one factor unlikely. Nevertheless, this study highlights a previously unappreciated role for ATP synthase in modulating the host immune response to *S. aureus* biofilm and infection persistence.

## MATERIALS AND METHODS

**Animals.** C57BL/6Ncr1 (RRID IMSR\_CRL:27), MyD88<sup>-/-</sup> (RRID IMSR\_JAX:009088), and TLR2<sup>-/-</sup> mice (RRID IMSR\_JAX:022507) were bred in-house at the University of Nebraska Medical Center (UNMC), and mice of the same sex were randomized into standard-density cages upon weaning ( $n = 5$  animals per cage). Mice were housed in a restricted-access biosafety level 2 (BSL2) room equipped with ventilated microisolator cages and maintained at 21°C under a 12-h light:12-h dark cycle with *ad libitum* access to water and chow with nestlets provided for enrichment. This study was conducted in strict accordance with the recommendations in the Guide for the Care and Use of Laboratory Animals of the National Institutes of Health. The protocol was approved by the UNMC Institutional Animal Care and Use Committee (18-013-03).

***S. aureus* strains.** The strains used in this study are described in Table S1. The *S. aureus* clinical isolate USA300 LAC 13C was cured of the LAC-p03 erythromycin (*erm*) resistance plasmid (23, 48) and is referred to as WT. The USA300 JE2 NTML strain  $\Delta$ *atpA* was moved to the LAC USA300 13C background via  $\phi$ 11 transduction as previously described (23). Strain background was validated by plasmid purification, and  $\Delta$ *atpA* was confirmed by growth on *erm* plates and PCR using *atpA*\_fwd and *atpA*\_rev primers (Table S1).

Chromosomal complementation of  $\Delta$ *atpA* was performed by replacing the transposon for the native gene using the allelic exchange plasmid pJB38 as previously described (49). Briefly, the *atpA* gene flanked with 1-kb arms was amplified using ATPase\_alpha\_C\_fwd and ATPase\_alpha\_C\_rev primers, and the shuttle vector was amplified using pJB38\_fwd and pJB38\_rev primers (Table S1). The resulting fragments were assembled using the NEBuilder HiFi DNA assembly cloning kit (New England Biolabs) to generate the pAQ67 plasmid that was electroporated into *E. coli* E10B. Subsequently, pAQ67 was electroporated into *S. aureus* RN4220 followed by transduction into  $\Delta$ *atpA* using  $\phi$ 11 to perform the allelic exchange process (49, 50). The  $\Delta$ *atpA* $\Delta$ *atl* strain was constructed by  $\phi$ 11 transduction of the NTML *atpA* mutation into a USA300 LAC 13C *atl* clean deletion mutant (*atl*) (51), with *atpA* and *atl* loss verified by PCR. To

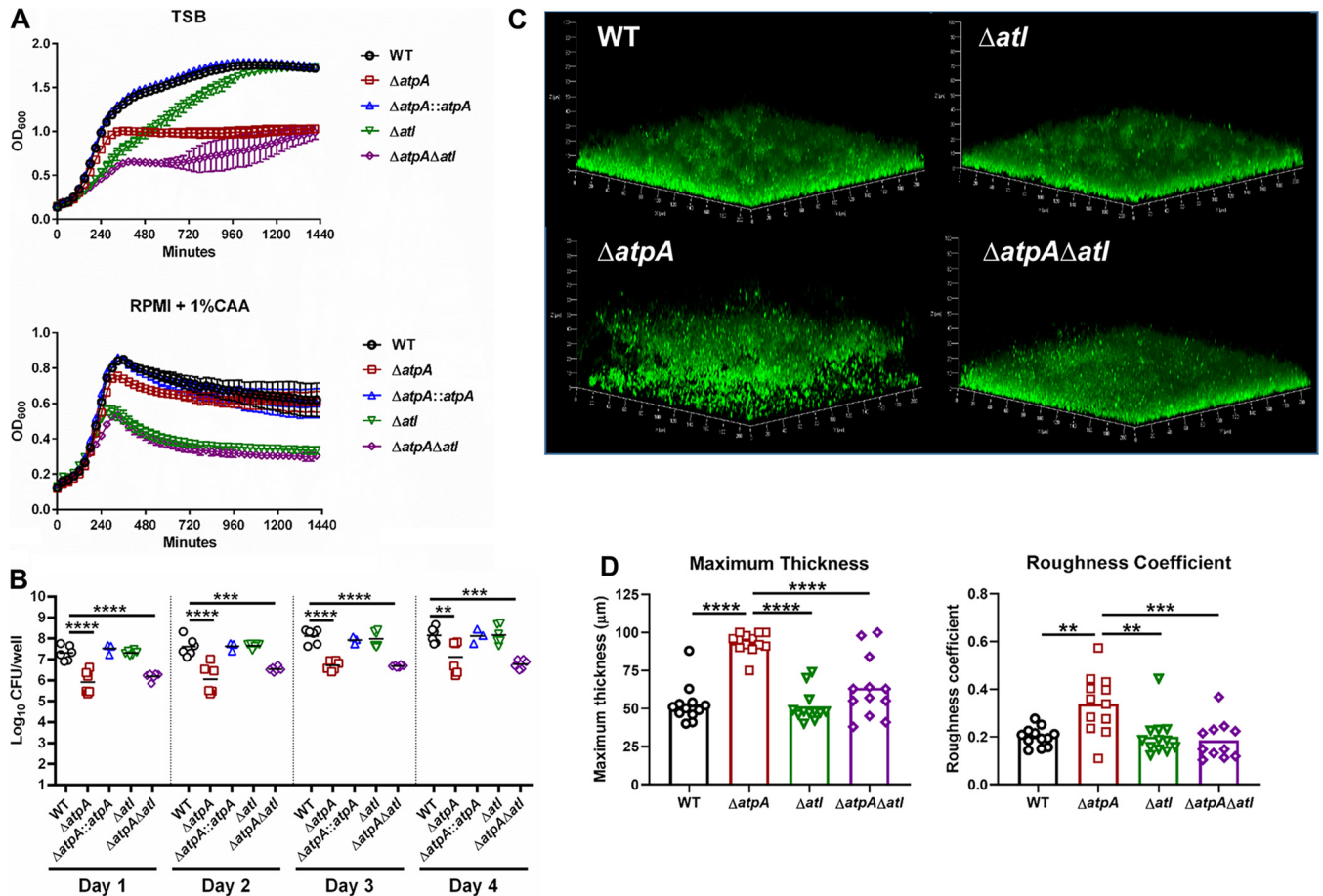


**FIG 10** AtI deletion reverses the aberrant morphology of *S. aureus*  $\Delta atpA$  biofilm. (A) OD<sub>600</sub> measurements of *S. aureus* strains in tryptic soy broth (TSB) or RPMI-1640 supplemented with 1% Casamino Acids (CAA) ( $n = 6$  biological replicates). (B) CFU of *in vitro* biofilms at various stages of maturation ( $n = 3$  to 6 biological replicates). (C) Representative 3D images of 4-day-old biofilm acquired using confocal laser scanning microscopy. (D) Maximum thickness and roughness coefficient measurements were calculated by Comstat 2 analysis combined from 2 independent experiments ( $n = 12$  biological replicates). Significant differences are denoted by asterisks (\*\*,  $P < 0.01$ , \*\*\*,  $P < 0.001$ , and \*\*\*\*,  $P < 0.0001$ ; one-way ANOVA with Dunnett's multiple-comparison test with WT control [B] or one-way ANOVA with Tukey's multiple-comparison test [D]).

visualize biofilm development, bacterial strains were transduced with pCM29-green fluorescent protein (GFP) (52) using  $\phi 11$  and confirmed by chloramphenicol resistance.

***S. aureus* planktonic and biofilm growth.** *S. aureus* strains were grown on Trypticase soy agar (TSA) with 5% sheep blood 1 day prior to the inoculation of broth cultures. For *in vitro* biofilm experiments, single colonies were added to 5 ml of RPMI-1640 supplemented with 1% CAA, 1% L-glutamine, and 1% HEPES (referred to as biofilm medium) and grown overnight at 37°C with constant shaking at 250 rpm for 16 to 18 h prior to use. Overnight cultures were diluted to an OD<sub>600</sub> of 0.05 for inoculation into 96-well and 12-well plates, or 8-well glass-bottom chamber slides (Thermo Fisher Nunc) that were previously coated with 20% human plasma in carbonate-bicarbonate buffer overnight at 4°C. Chloramphenicol (5  $\mu\text{g}/\text{ml}$ ) was added to biofilm medium for maintenance of the pCM29-GFP plasmid. Static biofilms were grown at 37°C with approximately 50% of medium replaced every 24 h. Where indicated, biofilms were treated with 100 U DNase or 10  $\mu\text{g}/\text{ml}$  of PAS beginning at the time of biofilm inoculation to assess the role of extracellular DNA or cell lysis, respectively, on MDSC and M $\Phi$  inflammatory properties.

Growth rates of *S. aureus* strains in liquid medium were determined using an Infinite Pro 200 (Tecan). Static biofilms were visualized using a Zeiss 710 META laser scanning confocal microscope (Carl Zeiss) at  $\times 40$  magnification. To obtain a representation of biofilm development and structure, z-stack images (0.88- $\mu\text{m}$  sections) were collected from 2 to 3 biological replicates (wells) for each strain, with results confirmed in 2 to 3 independent experiments. Maximum thickness and the dimensionless roughness coefficient of biofilms was determined using Comstat 2 (ImageJ) (53–55).

**MDSC and M $\Phi$  cultures.** Primary bone marrow-derived MDSCs and M $\Phi$ s were prepared from C57BL/6, MyD88<sup>-/-</sup>, or TLR2<sup>-/-</sup> mice as previously described (19, 22, 56). MDSCs were expanded for 4 days in RPMI-1640 supplemented with 10% fetal bovine serum (FBS), 1% L-glutamine, 1% HEPES, 1% antibiotic-antimitotic, 50  $\mu\text{M}$  beta-mercaptoethanol, 40 ng/ml GM-CSF, and 40 ng/ml G-CSF with 40 ng/ml IL-6 added at day 3 of culture. Following expansion, MDSCs were purified using an anti-Ly6G microbead kit (Miltenyi Biotec). M $\Phi$ s were propagated for 7 days in RPMI-1640 supplemented with 10%

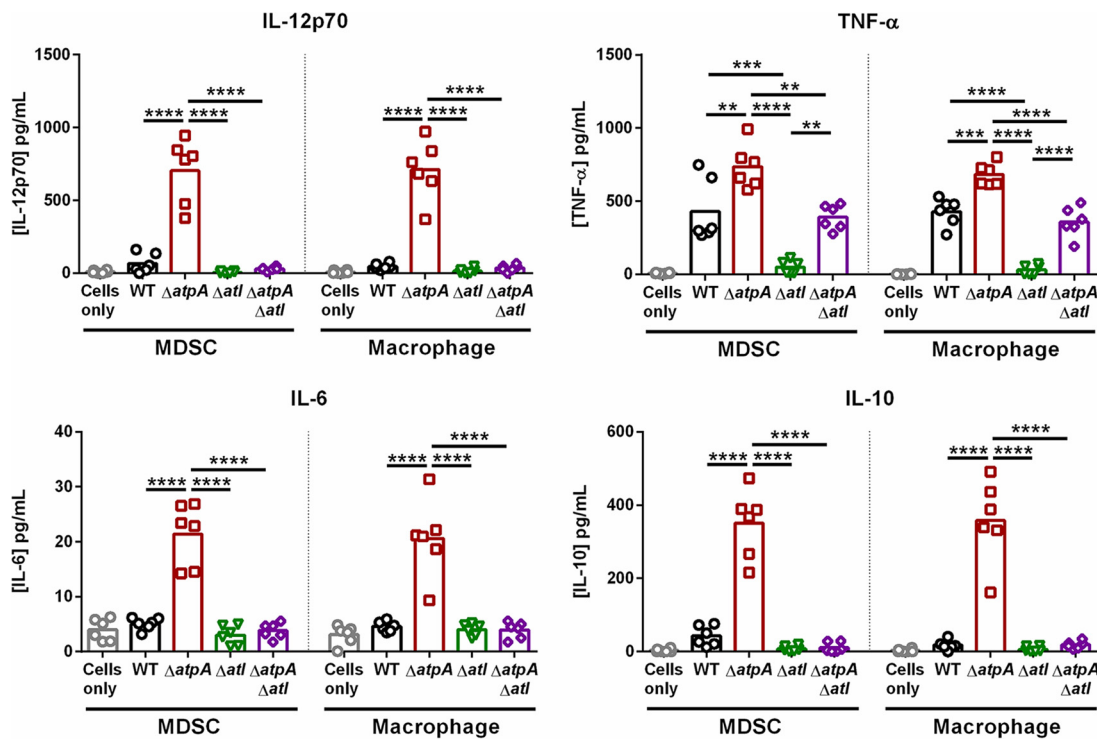


**FIG 11** *Atl* deletion prevents the enhanced cytokine response elicited by *S. aureus*  $\Delta atpA$  biofilm. Bone marrow-derived MDSCs or macrophages were cocultured with biofilm for 2 h, whereupon supernatants were analyzed using a mouse cytometric bead array inflammation kit. Results represent the mean combined from 2 independent experiments ( $n = 6$  biological replicates). Significant differences are denoted by asterisks (\*\*,  $P < 0.01$ , \*\*\*,  $P < 0.001$ , and \*\*\*\*,  $P < 0.0001$ ; one-way ANOVA with Tukey's multiple-comparison test).

FBS, 1% L-glutamine, 1% HEPES, 1% antibiotic-antimitotic, 50  $\mu M$  beta-mercaptoethanol, and 10% conditioned medium from L929 fibroblasts as a source of macrophage colony-stimulating factor (M-CSF) (28, 57). For visualizing M $\Phi$  invasion into biofilm by confocal microscopy, M $\Phi$ s were stained with CellTracker deep red (1  $\mu M$ ; Invitrogen) according to the manufacturer's instructions.

Human monocytes were obtained from healthy human donors by the UNMC Elutriation Core Facility by countercurrent centrifugal elutriation, in full compliance and with approval of the Institutional Review Board (IRB). Cells were cultured at  $1 \times 10^6$  cells/ml in RPMI-1640 supplemented with recombinant human M-CSF, 10% human serum, and 1% antibiotic-antimitotic for 7 days until harvest for experiments.

**Quantification of cytokine production by leukocytes following biofilm coculture.** MDSCs and M $\Phi$ s ( $5 \times 10^4$ /well) were cocultured with biofilm for 2 h at 37°C in a 96-well plate, whereupon plates were centrifuged and supernatants stored at  $-20^\circ C$  until analysis. Cytokine production was quantified using BD cytometric bead array mouse (catalog no. 552364) and human (catalog no. 551811) inflammation kits (both from BD Biosciences) according to the manufacturer's instructions and analyzed by flow cytometry using a BD LSR II.

**Gentamicin protection assay.** To determine whether *S. aureus*  $\Delta atpA$  was more susceptible to M $\Phi$  killing, a gentamicin protection assay was utilized. Overnight cultures of WT,  $\Delta atpA$ , and  $\Delta atpA::atpA$  were washed 1 time with PBS and incubated with M $\Phi$ s at a multiplicity of infection (MOI) of 1:1, 5:1, and 10:1 (bacteria:M $\Phi$ ) in a 96-well plate for 1 h at 37°C to allow for phagocytosis. After 1 h, plates were centrifuged, and fresh medium containing 100  $\mu g$ /ml gentamicin was added for 30 min at 37°C to kill residual extracellular bacteria. Next, fresh medium containing low-dose gentamicin (1  $\mu g$ /ml) was added, and M $\Phi$ s were incubated for various intervals over a 24-h period. At the indicated time points, M $\Phi$ s were lysed with 100  $\mu l$  sterile H $_2$ O followed by serial dilution on blood agar plates to quantify intracellular bacterial burden.

**Orthopedic implant model.** To evaluate the importance of *atpA* during biofilm development *in vivo*, a mouse model of *S. aureus* PJI was used as previously described (58). Since  $\Delta atpA$  had a postexponential-phase growth defect in TSB compared to WT, cultures were grown overnight at 37°C at 250 rpm and reinoculated at a starting OD $_{600}$  of 0.05 the following day and allowed to replicate for 4 h. There was no significant difference in the growth rate or number of viable bacteria following the 4-h subculture (Fig. S5). Sex- and age-matched C57BL/6NCRl mice (8 to 10 weeks old) were anesthetized with a ketamine/xylazine cocktail, and a medial parapatellar arthrotomy was performed to expose the distal femur. A burr hole was created in the femoral intercondylar notch using a 26-gauge needle, whereupon a 0.8-cm-long orthopedic-grade Kirschner wire (0.6 mm diameter, Nitinol [nickel-titanium]; Custom Wire

Technologies) was inserted into the intramedullary canal, leaving approximately 1 mm of the wire protruding into the joint space. Approximately  $10^3$  CFU of either WT,  $\Delta atpA$ , or  $\Delta atpA::atpA$  was inoculated into the joint cavity, with inocula verified the following day after growth on blood agar. The surgical site was sutured closed, and Buprenex (Reckitt Benckiser Health Care) was administered immediately following surgery and 24 h later for pain relief. Animals did not display any ambulatory defects or pain behaviors after this period and exhibited normal activity.

**Flow cytometry.** Leukocyte infiltrates into the surrounding soft tissue following *S. aureus* PJI were characterized using flow cytometry as previously described (59). Briefly, the soft tissue surrounding the knee joint was excised, disrupted using the blunt end of a 3-ml syringe plunger in PBS containing protease inhibitor (Thermo Scientific, Rockford, IL), and passed through a 70- $\mu$ m filter. Red blood cells (RBCs) were lysed using RBC lysis buffer (BioLegend, San Diego, CA), and the single-cell suspension was stained with CD11b-fluorescein isothiocyanate (FITC), CD45-allophycocyanin (APC), Ly6G-phycoerythrin (PE), Ly6C-peridinin chlorophyll protein (PerCP)-Cy5.5, F4/80-PE-Cy7 (BioLegend and BD Biosciences, San Diego, CA), and a Live/Dead fixable blue dead cell stain kit (Invitrogen, Eugene, OR) according to the manufacturers' instructions. Cell populations were analyzed using a BD LSR II and FACSDiva software (BD Bioscience, San Jose, CA), where MDSCs (CD11b<sup>high</sup> Ly6G<sup>+</sup> Ly6C<sup>+</sup> F4/80<sup>-</sup>), neutrophils (CD11b<sup>low</sup> Ly6G<sup>+</sup> Ly6C<sup>+</sup> F4/80<sup>-</sup>), monocytes (Ly6G<sup>-</sup> Ly6C<sup>+</sup> F4/80<sup>-</sup>), and M $\Phi$ s (Ly6G<sup>-</sup> Ly6C<sup>-</sup> F4/80<sup>+</sup>) are reported as the percentage of live CD45<sup>+</sup> cells.

**Multianalyte microbead array.** To quantify inflammatory mediator expression associated with WT and  $\Delta atpA$  PJI, homogenates prepared from the soft tissue surrounding the infected joint were analyzed using a Milliplex MAP mouse cytokine/chemokine magnetic bead panel (catalog no. MCYTMAP-70K-PX32; Millipore Sigma, Billerica, MA). Results were normalized to the total protein concentration per sample and bacterial burden to adjust for the differences in titer between WT and  $\Delta atpA$ -infected animals.

**Mass spectrometry.** The conditioned medium and cell extracts from WT and  $\Delta atpA$  biofilm were evaluated by LC-MS/MS to compare changes in the extracellular and intracellular proteome, respectively. WT and  $\Delta atpA$  biofilm were grown in 6-well plates as described above, whereupon supernatants were collected, centrifuged at 14,000 rpm for 10 min, and passed through a 0.2- $\mu$ m filter to remove any bacterial cells, followed by vacuum centrifugation to concentrate extracellular proteins. Biofilms were disrupted in cell lysis buffer (1 $\times$  PBS supplemented with 1 $\times$  protease inhibitor and one-half phosphatase inhibitor tablet [both from Thermo Fisher Scientific]) and lysed using a bead beater (Bullet Blender, Next Advance), and cell membranes were removed by centrifugation at 14,000 rpm for 10 min.

The protein concentration for each sample was determined using a bicinchoninic acid (BCA) protein assay kit (Pierce). Protein digestion for mass spectrometry and tandem mass tag (TMT) labeling of peptides were conducted following the manufacturer's recommendations. Briefly, 100  $\mu$ g of protein from each sample was reconstituted to 100  $\mu$ l with 100 mM triethylammonium bicarbonate (TEAB). Proteins were next reduced with 5  $\mu$ l of 200 mM tris (2-carboxyethyl) phosphine (TCEP) (1 h incubation at 55°C) and alkylated with 5  $\mu$ l of 375 mM iodoacetamide (IAA) for 30 min in the dark at room temperature (RT). The reduced and alkylated proteins were purified with acetone precipitation at -20°C overnight. The protein precipitates were collected by centrifugation at 8,000  $\times$  g for 10 min at 4°C, and the pellets were air-dried and resuspended in 100  $\mu$ l of 50 mM TEAB. Next, proteins were digested for 24 h at 37°C using 2.5  $\mu$ g of trypsin per sample. The amount of peptide yield in each sample was determined using a Pierce colorimetric peptide assay kit. The amounts of peptides to be tagged were normalized and mixed with 41  $\mu$ l of TMT reagent (TMTsixplex; Thermo Fisher Scientific) freshly dissolved in acetonitrile (ACN, 20  $\mu$ g/ $\mu$ l) for 1 h at RT, and the reaction was quenched with 8  $\mu$ l of 5% hydroxylamine (15 min incubation at RT). Tagged tryptic peptides were pooled and concentrated to ~20  $\mu$ l by vacuum centrifugation and analyzed using a high-resolution mass spectrometry nano-LC-MS/MS Tribrid system (Orbitrap Fusion Lumos coupled with an UltiMate 3000 high-performance liquid chromatography (HPLC) system; Thermo Scientific).

Approximately 800 ng of peptides were run on pre- (Acclaim PepMap 100, 75  $\mu$ m by 2 cm; nanoViper) and analytical columns (Acclaim PepMap RSLC, 75  $\mu$ m by 50 cm, nanoViper; both from Thermo Scientific). Peptides were eluted using a 125-min linear gradient of ACN (4 to 45%) in 0.1% fluorescent antibody (FA) and introduced to the mass spectrometer with a nanospray source. The MS scan was performed using the following detector settings: Orbitrap resolution, 120,000; scan range, 375 to 1,500  $m/z$ ; replicative-form (RF) lens, 60%; automatic gain control (AGC) target, 5.0E<sup>5</sup>; and maximum injection time, 150 ms. Ions with an intensity higher than 5.0E<sup>3</sup> and a charge state of 2 to 7 were selected in the MS scan for further fragmentation. MS2 scan parameters included collision-induced dissociation (CID) collision energy, 35%; activation Q, 0.25; AGC target, 1.0E<sup>4</sup>; and maximum injection time, 150 ms. MS3 scan parameters were high-energy collisional dissociation (HCD) collision energy, 65%; Orbitrap resolution, 50,000; scan range, 100 to 500  $m/z$ ; AGC target, 1.0E<sup>5</sup>; and maximum injection time, 200 ms.

All MS- and sequential mass spectrometry (MS<sup>n</sup>)-collected spectra were analyzed using a Protein Discoverer pipeline (version 2.1; Thermo Fisher Scientific). SEQUEST HT was used to search the Swiss-Prot database (selected for *S. aureus*, 2019\_03; 11,082 entries) using the following parameters: enzyme, trypsin; maximum missed cleavage, 2; precursor mass tolerance, 10 ppm; peptide tolerance,  $\pm$ 0.02 Da; fixed modifications (carbamidomethyl [C] and TMTsixplex [any N terminus]); and dynamic modifications (oxidation [M] and TMTsixplex [K]). The parameters for reporter ions quantifier were assigned as follows: integration tolerance, 20 ppm; integration method, most confident centroid; mass analyzer, FTMS (Fourier transform mass spectrometry); MS order, MS3; activation type, HCD; minimum collision energy,

0; and maximum collision energy, 1,000. A percolator was used to calculate the false discovery rate (FDR) for the peptide spectral matches using the following parameters: target FDR (strict), 0.01; target FDR (relaxed), 0.05; and validation based on  $q$  value. Quantification parameters were set as follows: peptides to use, unique; and normalization mode, total peptide amount. The complete set of differentially expressed proteins is presented in Data Set S1 and S2 in the supplemental material. Proteomaps (60) was used to generate Voronoi treemaps to visualize differentially expressed proteins in biofilm supernatant and extracts (Fig. S4).

**Extracellular DNA quantification.** eDNA isolation from static biofilms grown in 6-well plates was performed as described previously (61). Briefly, after 6 days of growth, biofilms were chilled to 4°C, 50 mM EDTA was added to the supernatant, and biofilms were mechanically disrupted in TES Buffer (Tris-HCl, pH 8.0, with 500 mM NaCl). Samples were subjected to subsequent phenol:chloroform:isoamyl alcohol (25:24:1) and chloroform:isoamyl alcohol (24:1) extractions and stored overnight at -20°C in 10% 3 M sodium acetate in EtOH. The next day, eDNA was pelleted by centrifugation and washed prior to resuspension in Tris-EDTA (TE) buffer. For eDNA quantification, qPCR for *gyrA* was performed using LightCycler DNA Master SYBR Green I (Roche).

**Statistics.** Significant differences were determined using a one- or two-way analysis of variance (ANOVA) with Tukey's or Dunnett's multiple comparisons, apart from the *in vivo* studies and gentamicin protection assay where significance between two groups was determined by a Student's  $t$  test with Holm-Sidak correction using GraphPad Prism version 6.04. Outliers were identified using a ROUT test ( $Q = 1\%$ ) in Prism. For all analyses,  $P < 0.05$  was considered statistically significant.

## SUPPLEMENTAL MATERIAL

Supplemental material is available online only.

**FIG S1**, TIF file, 0.3 MB.

**FIG S2**, TIF file, 0.1 MB.

**FIG S3**, TIF file, 0.1 MB.

**FIG S4**, TIF file, 1.7 MB.

**FIG S5**, TIF file, 0.2 MB.

**FIG S6**, TIF file, 0.2 MB.

**FIG S7**, TIF file, 0.1 MB.

**TABLE S1**, DOCX file, 0.02 MB.

**DATA SET S1**, XLSX file, 0.05 MB.

**DATA SET S2**, XLSX file, 0.1 MB.

## ACKNOWLEDGMENTS

This work was supported by the National Institutes of Health/National Institute of Allergy and Infectious Diseases grants P01AI083211 (project 4 to T.K.) and R01AI125588 to V.C.T.

We thank Rachel Fallet for managing the mouse colony and Vikas Kumar and Dragana Lagundzin in the UNMC Proteomics Core for performing the MS analysis. The UNMC Flow Cytometry Research Core receives support from The Fred & Pamela Buffett Cancer Center Support Grant (P30CA036727).

M.E.B., B.P.B., C.E.H., P.D.F., and T.K. designed experiments. M.E.B., B.P.B., C.E.H., and A.L.A. conducted experiments. A.A.A., S.S.C., and V.C.T. provided materials. M.E.B., B.P.B., and T.K. performed data curation. T.K. procured funding for this work. B.P.B. wrote the manuscript. All authors edited and approved the submission of this work.

We declare no conflicts of interest to report.

## REFERENCES

- Otto M. 2018. Staphylococcal biofilms. *Microbiol Spectr* 6. <https://doi.org/10.1128/microbiolspec.GPP3-0023-2018>.
- Tam K, Torres VJ. 2019. Staphylococcus aureus secreted toxins and extracellular enzymes. *Microbiol Spectr* 7. <https://doi.org/10.1128/microbiolspec.GPP3-0039-2018>.
- Foster TJ. 2005. Immune evasion by staphylococci. *Nat Rev Microbiol* 3:948–958. <https://doi.org/10.1038/nrmicro1289>.
- Askarian F, Wagner T, Johannessen M, Nizet V. 2018. Staphylococcus aureus modulation of innate immune responses through Toll-like (TLR), (NOD)-like (NLR) and C-type lectin (CLR) receptors. *FEMS Microbiol Rev* 42:656–671. <https://doi.org/10.1093/femsre/fuy025>.
- Kluytmans J, van Belkum A, Verbrugh H. 1997. Nasal carriage of Staphylococcus aureus: epidemiology, underlying mechanisms, and associated risks. *Clin Microbiol Rev* 10:505–520. <https://doi.org/10.1128/CMR.10.3.505-520.1997>.
- Krismer B, Weidenmaier C, Zipperer A, Peschel A. 2017. The commensal lifestyle of Staphylococcus aureus and its interactions with the nasal microbiota. *Nat Rev Microbiol* 15:675–687. <https://doi.org/10.1038/nrmicro.2017.104>.
- von Eiff C, Becker K, Machka K, Stammer H, Peters G. 2001. Nasal carriage as a source of Staphylococcus aureus bacteremia. *N Engl J Med* 344:11–16. <https://doi.org/10.1056/NEJM200101043440102>.
- Bode LGM, Kluytmans JAJW, Wertheim HFL, Bogaers D, Vandenbroucke-Grauls CMJE, Roosendaal R, Troelstra A, Box ATA, Voss A, van der Tweel I, van Belkum A, Verbrugh HA, Vos MC. 2010. Preventing surgical-site infections in nasal carriers of Staphylococcus aureus. *N Engl J Med* 362:9–17. <https://doi.org/10.1056/NEJMoa0808939>.



9. Ricciardi BF, Muthukrishnan G, Masters E, Ninomiya M, Lee CC, Schwarz EM. 2018. Staphylococcus aureus evasion of host immunity in the setting of prosthetic joint infection: biofilm and beyond. *Curr Rev Musculoskelet Med* 11:389–400. <https://doi.org/10.1007/s12178-018-9501-4>.
10. Kaplan SL. 2014. Recent lessons for the management of bone and joint infections. *J Infect* 68(Suppl 1):S51–S56. <https://doi.org/10.1016/j.jinf.2013.09.014>.
11. Zhu X, Sun X, Zeng Y, Feng W, Li J, Zeng J, Zeng Y. 2020. Can nasal Staphylococcus aureus screening and decolonization prior to elective total joint arthroplasty reduce surgical site and prosthesis-related infections? A systematic review and meta-analysis. *J Orthop Surg Res* 15:60–60. <https://doi.org/10.1186/s13018-020-01601-0>.
12. Romero-Palacios A, Petruccioli D, Main C, Winemaker M, de Beer J, Mertz D. 2020. Screening for and decolonization of Staphylococcus aureus carriers before total joint replacement is associated with lower S. aureus prosthetic joint infection rates. *American J Infection Control* 48:534–537. <https://doi.org/10.1016/j.ajic.2019.09.022>.
13. Donlan RM. 2001. Biofilms and device-associated infections. *Emerg Infect Dis* 7:277–281. <https://doi.org/10.3201/eid0702.010226>.
14. Gries CM, Kielian T. 2017. Staphylococcal biofilms and immune polarization during prosthetic joint infection. *J Am Acad Orthop Surg* 25(Suppl 1):S20–S24. <https://doi.org/10.5435/JAAOS-D-16-00636>.
15. Flemming H-C, Wingender J. 2010. The biofilm matrix. *Nat Rev Microbiol* 8:623–633. <https://doi.org/10.1038/nrmicro2415>.
16. Moormeier DE, Bayles KW. 2017. Staphylococcus aureus biofilm: a complex developmental organism. *Mol Microbiol* 104:365–376. <https://doi.org/10.1111/mmi.13634>.
17. Kumar A, Alam A, Rani M, Ehtesham NZ, Hasnain SE. 2017. Biofilms: survival and defense strategy for pathogens. *Int J Med Microbiol* 307:481–489. <https://doi.org/10.1016/j.jimm.2017.09.016>.
18. Heim CE, Vidlak D, Scherr TD, Koziel JA, Holzappel M, Muirhead DE, Kielian T. 2014. Myeloid-derived suppressor cells contribute to Staphylococcus aureus orthopedic biofilm infection. *J Immunol* 192:3778–3792. <https://doi.org/10.4049/jimmunol.1303408>.
19. Heim CE, Vidlak D, Kielian T. 2015. Interleukin-10 production by myeloid-derived suppressor cells contributes to bacterial persistence during Staphylococcus aureus orthopedic biofilm infection. *J Leukoc Biol* 98:1003–1013. <https://doi.org/10.1189/jlb.4VMA0315-125RR>.
20. Heim CE, Bosch ME, Yamada KJ, Aldrich AL, Chaudhari SS, Klinkebiel D, Gries CM, Alqarzaee AA, Li Y, Thomas VC, Seto E, Karpf AR, Kielian T. 2020. Lactate production by Staphylococcus aureus biofilm inhibits HDAC11 to reprogramme the host immune response during persistent infection. *Nat Microbiol* <https://doi.org/10.1038/s41564-020-0756-3>.
21. Heim CE, Vidlak D, Odvody J, Hartman CW, Garvin KL, Kielian T. 2018. Human prosthetic joint infections are associated with myeloid-derived suppressor cells (MDSCs): implications for infection persistence. *J Orthop Res* 36:1605–1613. <https://doi.org/10.1002/jor.23806>.
22. Heim CE, Vidlak D, Scherr TD, Hartman CW, Garvin KL, Kielian T. 2015. IL-12 promotes myeloid-derived suppressor cell recruitment and bacterial persistence during Staphylococcus aureus orthopedic implant infection. *J Immunol* 194:3861–3872. <https://doi.org/10.4049/jimmunol.1402689>.
23. Fey PD, Endres JL, Yajjala VK, Widhelm TJ, Boissy RJ, Bose JL, Bayles KW. 2013. A genetic resource for rapid and comprehensive phenotype screening of nonessential Staphylococcus aureus genes. *mBio* 4:e00537-12. <https://doi.org/10.1128/mBio.00537-12>.
24. Boyer PD. 1997. The ATP synthase—a splendid molecular machine. *Annu Rev Biochem* 66:717–749. <https://doi.org/10.1146/annurev.biochem.66.1.717>.
25. Deckers-Hebestreit G, Altendorf K. 1996. The F0F1-type ATP synthases of bacteria: structure and function of the F0 complex. *Annu Rev Microbiol* 50:791–824. <https://doi.org/10.1146/annurev.micro.50.1.791>.
26. Grosser MR, Paluscio E, Thurlow LR, Dillon MM, Cooper VS, Kawula TH, Richardson AR. 2018. Genetic requirements for Staphylococcus aureus nitric oxide resistance and virulence. *PLoS Pathog* 14:e1006907. <https://doi.org/10.1371/journal.ppat.1006907>.
27. Yamada KJ, Heim CE, Xi X, Attri KS, Wang D, Zhang W, Singh PK, Bronich TK, Kielian T. 2020. Monocyte metabolic reprogramming promotes pro-inflammatory activity and Staphylococcus aureus biofilm clearance. *PLoS Pathog* 16:e1008354. <https://doi.org/10.1371/journal.ppat.1008354>.
28. Hanke ML, Heim CE, Angle A, Sanderson SD, Kielian T. 2013. Targeting macrophage activation for the prevention and treatment of Staphylococcus aureus biofilm infections. *J Immunol* 190:2159–2168. <https://doi.org/10.4049/jimmunol.1202348>.
29. Thurlow LR, Hanke ML, Fritz T, Angle A, Aldrich A, Williams SH, Engenbretsen IL, Bayles KW, Horswill AR, Kielian T. 2011. Staphylococcus aureus biofilms prevent macrophage phagocytosis and attenuate inflammation in vivo. *J Immunol* 186:6585–6596. <https://doi.org/10.4049/jimmunol.1002794>.
30. Takeuchi O, Hoshino K, Akira S. 2000. Cutting edge: TLR2-deficient and MyD88-deficient mice are highly susceptible to Staphylococcus aureus infection. *J Immunology* 165:5392–5396. <https://doi.org/10.4049/jimmunol.165.10.5392>.
31. Pietrocola G, Arciola CR, Rindi S, Di Poto A, Missineo A, Montanaro L, Speziale P. 2011. Toll-like receptors (TLRs) in innate immune defense against Staphylococcus aureus. *Int J Artif Organs* 34:799–810. <https://doi.org/10.5301/ijao.5000030>.
32. Okshevsky M, Meyer RL. 2015. The role of extracellular DNA in the establishment, maintenance and perpetuation of bacterial biofilms. *Crit Rev Microbiol* 41:341–352. <https://doi.org/10.3109/1040841X.2013.841639>.
33. Wecke J, Lahav M, Ginsburg I, Kwa E, Giesbrecht P. 1986. Inhibition of wall autolysis of staphylococci by sodium polyanethole sulfonate “liquid”. *Arch Microbiol* 144:110–115. <https://doi.org/10.1007/BF00414719>.
34. Biswas R, Biswas L, Simon U, Hentschel P, Thumm G, Götz F. 2006. Activity of the major staphylococcal autolysin Atl. *FEMS Microbiol Lett* 259:260–268. <https://doi.org/10.1111/j.1574-6968.2006.00281.x>.
35. Houston P, Rowe SE, Pozzi C, Waters EM, Gara JP. 2011. Essential role for the major autolysin in the fibronectin-binding protein-mediated Staphylococcus aureus biofilm phenotype. *Infect Immun* 79:1153–1165. <https://doi.org/10.1128/IAI.00364-10>.
36. Vestergaard M, Leng B, Haaber J, Bojer MS, Vegge CS, Ingmer H. 2016. Genome-wide identification of antimicrobial intrinsic resistance determinants in Staphylococcus aureus. *Front Microbiol* 7:2018. <https://doi.org/10.3389/fmicb.2016.02018>.
37. Vestergaard M, Nøhr-Meldgaard K, Bojer MS, Krogsgård Nielsen C, Meyer RL, Slavetinsky C, Peschel A, Ingmer H. 2017. Inhibition of the ATP synthase eliminates the intrinsic resistance of Staphylococcus aureus towards polymyxins. *mBio* 8:e01114-17. <https://doi.org/10.1128/mBio.01114-17>.
38. Graczyk JP, Harvey CJ, Laczko V, Alonzo F, III. 2017. A lipoylated metabolic protein released by Staphylococcus aureus suppresses macrophage activation. *Cell Host Microbe* 22:678–687.e9. <https://doi.org/10.1016/j.chom.2017.09.004>.
39. Conlon BP, Rowe SE, Lewis K. 2015. Persister cells in biofilm associated infections, p 1–9. *In* Donelli G (ed), *Biofilm-based healthcare-associated infections*, vol. II. Springer International Publishing, Cham, Switzerland. [https://doi.org/10.1007/978-3-319-09782-4\\_1](https://doi.org/10.1007/978-3-319-09782-4_1).
40. Balaban NQ, Helaine S, Lewis K, Ackermann M, Aldridge B, Andersson DI, Brynildsen MP, Bumann D, Camilli A, Collins JJ, Dehio C, Fortune S, Ghigo J-M, Hardt W-D, Harms A, Heinemann M, Hung DT, Jenal U, Levin BR, Michiels J, Storz G, Tan M-W, Tenson T, Van Melderen L, Zinkernagel A. 2019. Definitions and guidelines for research on antibiotic persistence. *Nat Rev Microbiol* 17:441–448. <https://doi.org/10.1038/s41579-019-0196-3>.
41. Conlon BP, Rowe SE, Gandt AB, Nuxoll AS, Donegan NP, Zalis EA, Clair G, Adkins JN, Cheung AL, Lewis K. 2016. Persister formation in Staphylococcus aureus is associated with ATP depletion. *Nat Microbiol* 1:16051. <https://doi.org/10.1038/nmicrobiol.2016.51>.
42. Scherr TD, Hanke ML, Huang O, James DB, Horswill AR, Bayles KW, Fey PD, Torres VJ, Kielian T. 2015. Staphylococcus aureus biofilms induce macrophage dysfunction through leukocidin AB and alpha-toxin. *mBio* 6:e01021-15. <https://doi.org/10.1128/mBio.01021-15>.
43. Marongiu L, Gornati L, Artuso I, Zanoni I, Granucci F. 2019. Below the surface: the inner lives of TLR4 and TLR9. *J Leukoc Biol* 106:147–160. <https://doi.org/10.1002/JLB.3MIR1218-483RR>.
44. Alonzo F, III, Torres VJ. 2014. The bicomponent pore-forming leucocidins of Staphylococcus aureus. *Microbiol Mol Biol Rev* 78:199–230. <https://doi.org/10.1128/MMBR.00055-13>.
45. DuMont AL, Yoong P, Liu X, Day CJ, Chumblor NM, James DB, Alonzo F, III, Bode NJ, Lacy DB, Jennings MP, Torres VJ. 2014. Identification of a crucial residue required for Staphylococcus aureus LukAB cytotoxicity and receptor recognition. *Infect Immun* 82:1268–1276. <https://doi.org/10.1128/IAI.01444-13>.
46. Bhakdi S, Tranum-Jensen J. 1991. Alpha-toxin of Staphylococcus aureus. *Microbiol Rev* 55:733–751. <https://doi.org/10.1128/MMBR.55.4.733-751.1991>.
47. Yoong P, Torres VJ. 2013. The effects of Staphylococcus aureus leukotoxins on the host: cell lysis and beyond. *Curr Opin Microbiol* 16:63–69. <https://doi.org/10.1016/j.mib.2013.01.012>.

48. Kennedy AD, Porcella SF, Martens C, Whitney AR, Braughton KR, Chen L, Craig CT, Tenover FC, Kreiswirth BN, Musser JM, DeLeo FR. 2010. Complete nucleotide sequence analysis of plasmids in strains of *Staphylococcus aureus* clone USA300 reveals a high level of identity among isolates with closely related core genome sequences. *J Clin Microbiol* 48:4504–4511. <https://doi.org/10.1128/JCM.01050-10>.
49. Bose JL, Fey PD, Bayles KW. 2013. Genetic tools to enhance the study of gene function and regulation in *Staphylococcus aureus*. *Appl Environ Microbiol* 79:2218–2224. <https://doi.org/10.1128/AEM.00136-13>.
50. Kreiswirth BN, Lofdahl S, Betley MJ, O'Reilly M, Schlievert PM, Bergdoll MS, Novick RP. 1983. The toxic shock syndrome exotoxin structural gene is not detectably transmitted by a prophage. *Nature* 305:709–712. <https://doi.org/10.1038/305709a0>.
51. Bose JL, Lehman MK, Fey PD, Bayles KW. 2012. Contribution of the *Staphylococcus aureus* Atl AM and GL murein hydrolase activities in cell division, autolysis, and biofilm formation. *PLoS One* 7:e42244. <https://doi.org/10.1371/journal.pone.0042244>.
52. Mootz JM, Malone CL, Shaw LN, Horswill AR. 2013. Staphopains modulate *Staphylococcus aureus* biofilm integrity. *Infect Immun* 81:3227–3238. <https://doi.org/10.1128/IAI.00377-13>.
53. Heydorn A, Nielsen AT, Hentzer M, Sternberg C, Givskov M, Ersboll BK, Molin S. 2000. Quantification of biofilm structures by the novel computer program Comstat. *Microbiology* 146:2395–2407. <https://doi.org/10.1099/00221287-146-10-2395>.
54. Vorregaard M. 2008. Comstat2 - a modern 3D image analysis environment for biofilms. Informatics and Mathematical Modelling, Technical University of Denmark, Kongens Lyngby, Denmark.
55. Schneider CA, Rasband WS, Eliceiri KW. 2012. NIH Image to ImageJ: 25 years of image analysis. *Nat Methods* 9:671–675. <https://doi.org/10.1038/nmeth.2089>.
56. Yamada KJ, Heim CE, Aldrich AL, Gries CM, Staudacher AG, Kielian T. 2018. Arginase-1 expression in myeloid cells regulates *Staphylococcus aureus* planktonic but not biofilm infection. *Infect Immun* 86:e00206-18. <https://doi.org/10.1128/IAI.00206-18>.
57. Kigerl KA, Gensel JC, Ankeny DP, Alexander JK, Donnelly DJ, Popovich PG. 2009. Identification of two distinct macrophage subsets with divergent effects causing either neurotoxicity or regeneration in the injured mouse spinal cord. *J Neurosci* 29:13435–13444. <https://doi.org/10.1523/JNEUROSCI.3257-09.2009>.
58. Bernthal NM, Stavrakis AI, Billi F, Cho JS, Kremen TJ, Simon SI, Cheung AL, Finerman GA, Lieberman JR, Adams JS, Miller LS. 2010. A mouse model of post-arthroplasty *Staphylococcus aureus* joint infection to evaluate in vivo the efficacy of antimicrobial implant coatings. *PLoS One* 5:e12580. <https://doi.org/10.1371/journal.pone.0012580>.
59. Heim CE, West SC, Ali H, Kielian T. 2018. Heterogeneity of Ly6G(+) Ly6C(+) myeloid-derived suppressor cell infiltrates during *Staphylococcus aureus* biofilm infection. *Infect Immun* 86. <https://doi.org/10.1128/IAI.00684-18>.
60. Liebermeister W, Noor E, Flamholz A, Davidi D, Bernhardt J, Milo R. 2014. Visual account of protein investment in cellular functions. *Proc Natl Acad Sci U S A* 111:8488–8493. <https://doi.org/10.1073/pnas.1314810111>.
61. Rice KC, Mann EE, Endres JL, Weiss EC, Cassat JE, Smeltzer MS, Bayles KW. 2007. The cidA murein hydrolase regulator contributes to DNA release and biofilm development in *Staphylococcus aureus*. *Proc Natl Acad Sci U S A* 104:8113–8118. <https://doi.org/10.1073/pnas.0610226104>.